

Review

Merging Metallic Catalysts and Sonication: A Periodic Table Overview

Claudia E. Domini ¹, Mónica B. Álvarez ¹, Gustavo F. Silbestri ^{1,*}, Giancarlo Cravotto ² and Pedro Cintas ^{3,*}

¹ Instituto de Química del Sur (INQUISUR), Departamento de Química, Universidad Nacional del Sur (UNS)-Consejo Nacional de Investigaciones Científicas y Técnicas (CONICET), Avenida Alem 1253, Bahía Blanca 8000, Argentina; claudia.domini@uns.edu.ar (C.E.D.); monica.alvarez@uns.edu.ar (M.B.Á.)

² Dipartimento di Scienza e Tecnologia del Farmaco, University of Turin, Via P. Giuria 9, 10125 Turin, Italy; giancarlo.cravotto@unito.it

³ Departamento de Química Orgánica e Inorgánica, Facultad de Ciencias-Universidad de Extremadura, and Instituto del Agua, Cambio Climático y Sostenibilidad (IACYS)-Unidad de Química Verde y Desarrollo Sostenible, Avda. de Elvas s/n, 06006 Badajoz, Spain

* Correspondence: gsilbestri@uns.edu.ar (G.F.S.); pecintas@unex.es (P.C.); Tel.: +54-291-459-5101 (G.F.S.); Tel.: +34-924-289-300 (P.C.)

Academic Editor: Keith Hohn

Received: 8 March 2017; Accepted: 14 April 2017; Published: 19 April 2017

Abstract: This account summarizes and discusses recent examples in which the combination of ultrasonic waves and metal-based reagents, including metal nanoparticles, has proven to be a useful choice in synthetic planning. Not only does sonication often enhance the activity of the metal catalyst/reagent, but it also greatly enhances the synthetic transformation that can be conducted under milder conditions relative to conventional protocols. For the sake of clarity, we have adopted a structure according to the periodic-table elements or families, distinguishing between bulk metal reagents and nanoparticles, as well as the supported variations, thus illustrating the characteristics of the method under consideration in target synthesis. The coverage focuses essentially on the last decade, although the discussion also strikes a comparative balance between the more recent advancements and past literature.

Keywords: metal catalysts; nanoparticles; organic synthesis; sonication; supported metal reagent/catalyst; ultrasound

1. Introduction

The interaction of ultrasound with metals dates back to early sonochemistry, from the 1950s onwards, when some scientists discovered, rather by serendipity, that organometallic reagents and their subsequent coupling with organic compounds could be greatly improved by sonication in ultrasonic baths. The method clearly rivaled traditional procedures employed for metal reagents, as the ultrasonic protocol worked well without inert conditions and undried solvents. These pluses were initially associated to cleaning effects that removed the passivating coat of the otherwise unreactive zero-valent metals. There has been considerable progress since, and the reader is referred to past and recent major reviews that document in detail the mechanisms involved in activation of metal surfaces, notably by creating reactive sites by atomic dislocation and corrosion effects, as well as facile metalations and further reactions with an organic compound [1–5]. Of major significance in this context is the use of sonication in Barbier and Barbier-like reactions, where tedious and complex operations required to activate bulk metals are usually converted into simpler one-pot reactions [6,7].

The activation also applies to metal nanoparticles (NPs) [8–10], although their stability and reactivity may be substantially different from those of bulk metals, even though finely divided, and often require polymeric additives and/or deposition on inert supports, thus increasing the lifetimes of NPs in solution.

Electron microscopy and X-ray diffraction reveal morphological surface changes induced by sonication on the crystal structure of metals such as Al, Cu, Zn, or Ag, which exhibit different hardness and natural roughness. As expected, cavitation plays a pivotal role, especially through mechanical effects generated by the collapse of microbubbles and the action of shock waves on a given surface. Both damage and deformation translate into structural reorganization of crystallites leading to small dimensional variations, weak grain cohesion, and atomic defects [11]. Chemical effects, especially surface oxidation induced by reactive species formed by substrate or solvent pyrolysis and released after bubble implosion, also contribute to structural changes of metal surfaces [12].

It is now well established that effects caused by cavitation can globally be rationalized by assuming a spherical model of bubbles, as microreactors, where three sonochemical reaction zones are identified [13]. The core or inner environment provides high local temperatures and pressures for volatile solutes capable of entering into the bubble and undergoing such intense conditions when it collapses. Given the extremely fast collapse and concomitant cooling rates (exceeding 10^{10} K per second), the structural reorganization and/or crystallization is highly hindered, thereby resulting in amorphous products. The interfacial region, between the core and the surrounding liquid, provides less intense conditions, yet high enough—ca. 1900 K—to bring about a chemical reaction. The interfacial region appears to be the prevalent zone where non-volatile substrates or those unable to enter into the bubble may react. Given the fast kinetics of collapse, the growth of the nuclei will also be considerably restricted and this may result in nanostructured or nanocrystalline materials depending on the temperature. The third zone comprising the bulk liquid at ambient conditions can also be the site for sonochemical reactions to occur, notably after releasing of reactive species generated by bubble collapse. However, the formation rate will also be lower [14].

The interplay between ultrasonic irradiation and metal activation can also be regarded within the green chemistry domain, even if some metal particles are inherently toxic materials and organic solvents cannot be completely avoided. However, these drawbacks are more than compensated for by the milder, faster, and more efficient processes run under sonication. Aqueous environments are often tolerated and new mechanistic pathways may afford functionalized derivatives not attained by thermal activation, thus switching conventional routes. In addition, it is worth pointing out that ultrasound along with other sustainable and enabling technologies provide sufficient activation to perform chemical reactions under solvent-free (i.e., neat reagents) and catalyst-free conditions [15].

This perspective is aimed at providing a good coverage of recent developments in the use of metal derivatives and metal NPs, generated and manipulated under ultrasound, hoping to be illustrative enough of the breadth and strength of the technique. The goals are focused on the capture of fundamental details that make ultrasound advantageous in a particular catalytic application. The preparation of micro- and nanomaterials with potential catalytic activity has grown almost exponentially. Since our analysis cannot be overlong, thus aiding readability and outlook of the applications presented, the article is largely restricted to synthetic strategies and/or specific applications, i.e., the sonochemical preparation of metal nanostructures or metal NPs without such detailed explorations cannot be treated, apart from a few exceptions in terms of discussion or comparative purposes. Accordingly, the authors hope to marry the properties of concision and representative cases, yet being informative and insightful.

2. Transition Metals and Supported Transition Metal Reagents

The use of transition metals still represents the main domain of applications in synthesis and catalysis aided by ultrasound. Metal powders or metal alloys as well as other non-zero valent precursors, cheap metal oxides or metal halides for instance, are usually employed as precursors and

An improved sonochemical protocol also developed by the Cravotto group employs commercially available Cu turnings as catalyst [21]. Ultrasound smoothly triggered the redox process between metallic Cu and Cu(II) oxide on the metal surface leading to Cu(I) species. This protocol is much simpler and inexpensive than other catalysts employed for CuAAC reactions and works well in water, where the latter itself serves as ligand and metallic wastes are easily removed by filtration. As depicted in Figure 1, both sonication alone (with a Ti horn) and simultaneous MW/US (pyrex horn) can be successfully employed [21,22].

Table 1. Cu-catalyzed alkyne-azide cycloaddition (CuAAC) reactions activated under different thermal conditions.

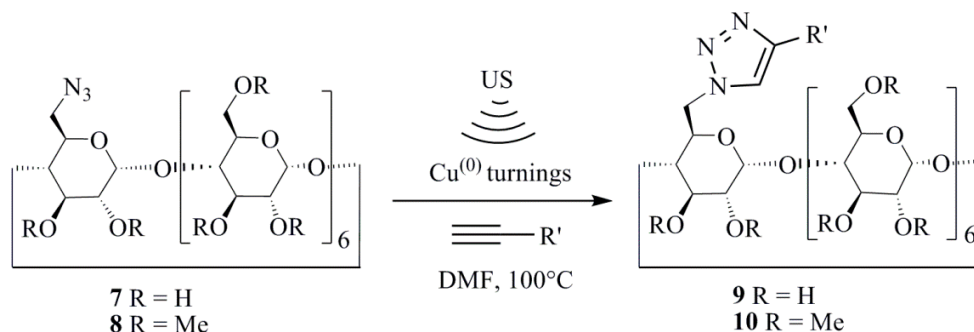
Catalyst (10 mol %)	Conditions (at 85 °C)	Reaction Time	Yield (%)
Cu(II)/C, L-ascorbic acid ^(a)	oil bath	2 h	79
Cu(II)/C, L-ascorbic acid	MW	10 min	83
recycled Cu(II)/C ^(b)	MW	30 min	84
Cu(II)/C	oil bath	3 h	30
Cu(II)/C	MW	45 min	81
Cu(I)/C	oil bath	2 h	78
Cu(I)/C	MW	10 min	89
Cu(I)/C	MW/US	10 min	93

^(a) C = charcoal. ^(b) Catalyst recycled from the above reaction.



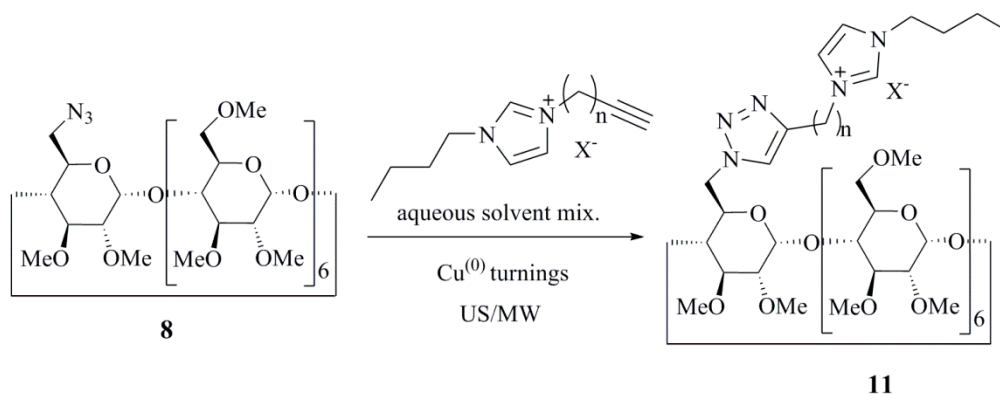
Figure 1. Click cycloadditions with metallic copper activated by ultrasound alone (**left**) and the combined action of US and MW irradiations in a professional MW reactor (**right**). Set-ups from Cravotto's group laboratory at the University of Turin.

An advantageous application of the above procedure deals with the structural modification of cyclodextrins, which constitute versatile ligands and scaffolds in supramolecular chemistry, as well as stationary phases in chiral chromatography. Cyclodextrins form stable sandwich-type inclusion compounds with copper ions, giving rise to a green-grayish coloration that require time-consuming purifications using chelate agents [23]. Metallic copper as catalyst in dimethylformamide (DMF) at high temperature affords cyclodextrin-triazole derivatives (**9** and **10**, Scheme 3) as white powders, with only trace amounts of the metal [22].



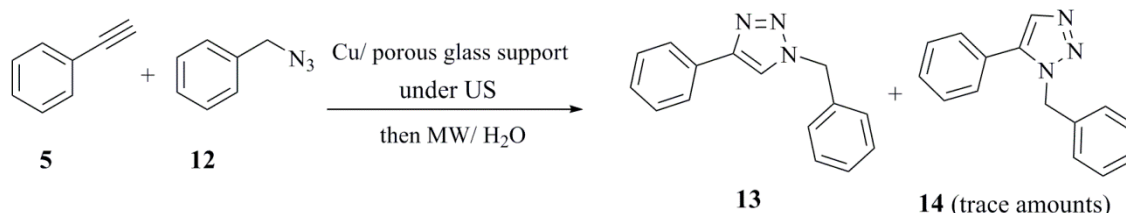
Scheme 3. CuAAC reactions in the presence of Cu(0) with β -cyclodextrin derivatives as substrates.

Further extension of the same conceptual basis to imidazolium-functionalized alkynes led to positively charged triazole-bridged cyclodextrins (Scheme 4), which exhibit hybrid properties of cyclodextrins as encapsulating hosts and ionic liquids [24]. This transformation can be conducted in an aqueous environment and is more efficient under the simultaneous action of US/MW irradiation.



Scheme 4. CuAAC leading to hybrid cyclodextrin-triazole-based ionic liquids.

Jacob et al. developed porous glasses as a novel catalyst support for CuAAC reactions. The catalyst could easily be generated by sonication in 5–10 min from Cu(II) acetate in aqueous medium using an ultrasonic bath. The calcined catalyst was then employed in the click cycloaddition under MW-assisted heating (Scheme 5) [25]. This resulted in excellent regioselectivity and yields within short reaction times. The experimental conditions were optimized using the cycloaddition of phenylacetylene (5) and benzyl azide (12). Recyclability studies also showed that the catalyst could be reused up to four times with comparable efficiency.



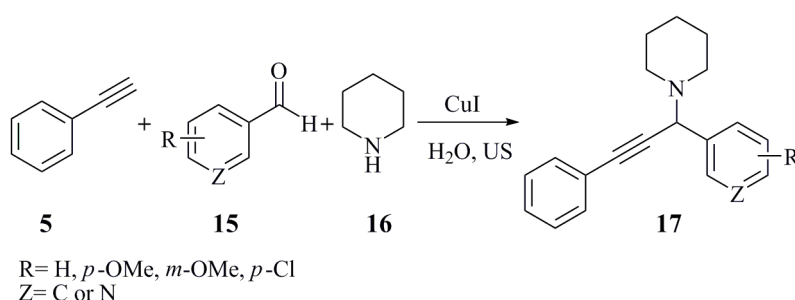
Scheme 5. Click-reaction using a porous glass support.

With the advent and development of flow processes, which not only avoid hazards on manipulating toxic substances, but also miniaturization and intensification, an interesting click reaction in continuous flow has also been reported [26]. The reactor in question consists of a copper-made

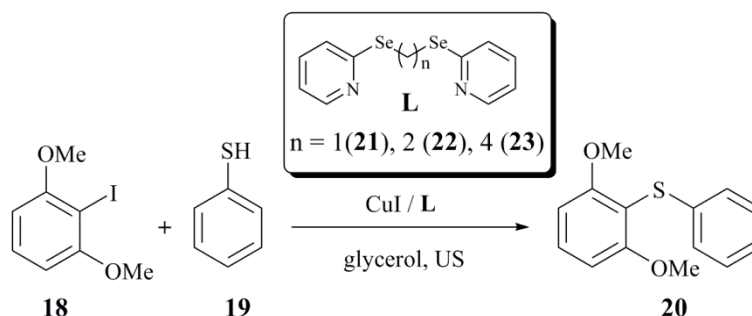
cassette that integrates a piezoelectric transducer. 1,4-Disubstituted triazoles were obtained in yields ranging from 15% to 55% and within 50–150 °C depending on the starting substrates in only 5–10 min.

Couplings other than alkyne-azide cycloadditions mediated by Cu species and activated by sonication have also proven to be useful in synthesis. Thus, ultrasonic irradiation was applied to the addition of metal acetylides to in situ generated imines leading to propargylamines (**17**), a protocol described more than one decade ago (Scheme 6). Even though the process was conducted in a common ultrasonic bath, good yields were obtained at room temperature using CuI in aqueous solution [27].

More recently, Cargnelutti et al. described a straightforward C-S coupling of aryl halides (**18**) with thiols (**19**) in glycerol, catalyzed by CuI/bis(2-pyridyl)diselenoethers and using ultrasound (as alternative energy source) to accelerate the process (Scheme 7) [28]. The efficiency of such C-S couplings in glycerol is analogous to other cross-coupling reactions in toxic organic solvents, which also employ more expensive catalysts based on transition metals. The method allowed the use of a wide range of functionalized reaction partners, giving the desired products in good yields.



Scheme 6. Cu(I)-mediated synthesis of propargylamines.



Scheme 7. Synthesis of aryl sulfides using bis(2-pyridyl)diselenoethers.

Cheaper and abundant transition metals invariably represent valuable resources for metal-assisted transformations. Pirola et al. prepared supported iron catalysts for Fischer-Tropsch (FT) reactions using different methods, both conventional and non-conventional [29]. Metal deposition on silica was conducted with either ultrasound (US) or microwave (MW), thereby increasing the catalyst activity. Data obtained for FT reactions showed that the catalysts generated under sonication were the most efficient, especially under an inert (Ar) atmosphere. MW-prepared catalysts afforded results comparable to those obtained with conventional protocols.

Copper chromite (with formula $\text{Cu}_2\text{Cr}_2\text{O}_5$), sometimes referred to as the Adkins catalyst, and TiO_2 -supported copper chromite catalysts have been prepared by means of different methods, and their catalytic performance assessed in the liquid-phase hydrogenation of furfural giving rise to furfuryl alcohol [30]. TiO_2 -supported catalysts obtained under ultrasonication exhibited the highest activity. Notably, the catalytic activity was dependent on the temperature and studies conducted at 140, 170, and 200 °C showed the best results at the lowest temperature. The catalyst's efficiency was ascribed to the amount of reducible Cu(II) ions present in the catalyst and the metallic surface.

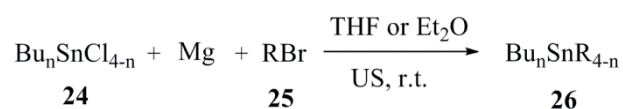
Cu(0) was generated by reduction of the catalyst with H₂. The activity was completely lost when carbon deposited on the surface or decreased the amount of metal species.

Arena et al. also conducted a systematic research on the effects of Zn/Cu ratios on the structure and adsorption of Cu–ZnO/ZrO₂ catalysts (Zn/Cu ratios = 0–3; ZrO₂ = 42–44 wt %), synthesized via the reverse co-precipitation under ultrasound energy. Cu/ZrO₂ and Cu–ZnO/ZrO₂ systems ensured a superior activity in the hydrogenation reaction of CO₂ to methanol with respect to conventional catalysts [31].

3. Main Group Metal Derivatives

Unlike zero-valent transition metals, some exhibiting high hardness and being reluctant to undergo a direct metalation process [1,5], some main group elements, especially Group 13 and 14 metals, often show characteristics typical of alkaline or alkaline-earth elements and can also tolerate hydrophilic media and sensitive functional groups. Both metalation and couplings can be smoothly conducted under the action of ultrasound waves. It suffices, for instance, to mention that organostannane compounds (alkyl, alkenyl, and aryl derivatives), which are typically prepared by transmetalation of the corresponding Grignard or organolithium reagents with bis(tributyltin) oxide, can however be synthesized via a direct Barbier-like reaction under sonication [32,33]. A similar strategy employing germanium halides, Mg turnings, and organohalides under sonication enables the preparation of the corresponding organogermanium compounds [34].

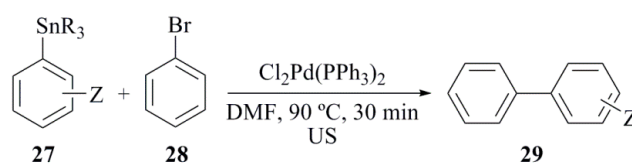
Despite their toxicity, organostannates are versatile reagents to accomplish a variety of metal-mediated couplings, the Stille reaction in particular. In 2009 Lamandé-Langle et al. described a general procedure that allows the efficient synthesis of various organotin compounds in following a Barbier-like strategy as well (Scheme 8) [35]. The process offers a number of advantages such as simplicity and good yields, and reagent quality (both solvents and tin halides) does not constitute a critical issue. Moreover, careful purification before use and the presence of an additive are not required. Numerous organotin compounds could easily be synthesized in a simplified and improved one-step ultrasound-assisted Barbier reaction via cross-coupling of a variety of organic bromides (25) with stannyl chlorides (24: Bu₃SnCl, Bu₂SnCl₂, BuSnCl₃, SnCl₄) promoted by magnesium. The di- and tri-functional derivatives (26) were further used in a Stille cross-coupling reaction, with different iodovinyl acids (or esters) to determine how many groups were transferred.



R = Alkyl, Allyl, Alkenyl, Allenyl, Aryl, N-Aryl

Scheme 8. Sonochemical synthesis of organotin compounds.

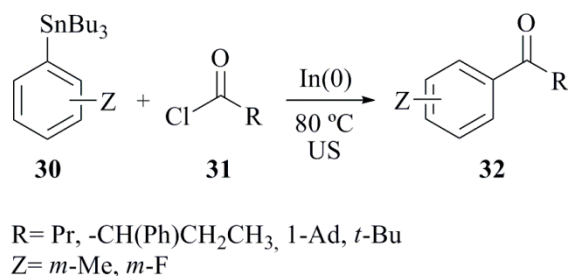
In 2012, Domini et al. reported an improved Stille synthesis of unsymmetrical biaryls (29) when conducting the coupling under sonication (Scheme 9) [36]. Yields ranged from 57% to 97% in 30 min, whereas the silent transformation took ca. 20 h to afford similar results.



R = Me, Bu
Z = *o*-OMe, *m*-OMe, *p*-OMe, *m*-Me, *m*-Cl

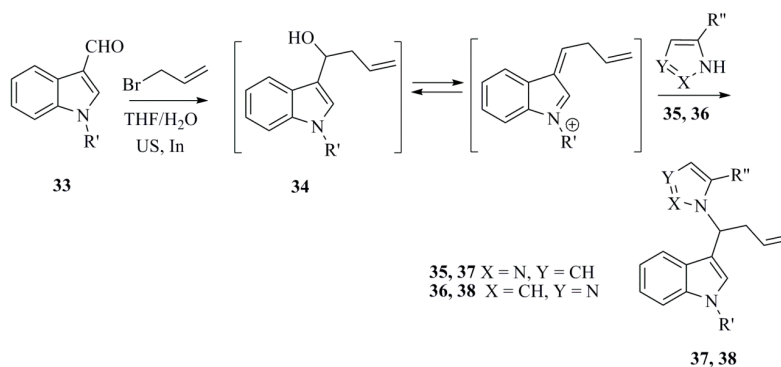
Scheme 9. Synthesis of unsymmetrical biaryls.

Arylstannanes (**30**) have been recently employed as useful partners with alkanoyl chlorides (**31**) in an indium-mediated regioselective synthesis of alkyl aryl ketones (**32**) (Scheme 10) [37]. The protocol also works for aryl vinyl ketones. Yields were moderate to good (42–84%) and, remarkably, the transformation can be run under neat conditions, without requiring an organic solvent. Sonication dramatically reduced the reaction times compared to conventional conditions (from 3–32 h to 10–70 min depending on the starting materials). Indium appears to be a radical initiator and the authors suggest a catalytic cycle involving a single-electron transfer (SET) mechanism.



Scheme 10. Indium-mediated regioselective synthesis of alkyl aryl ketones.

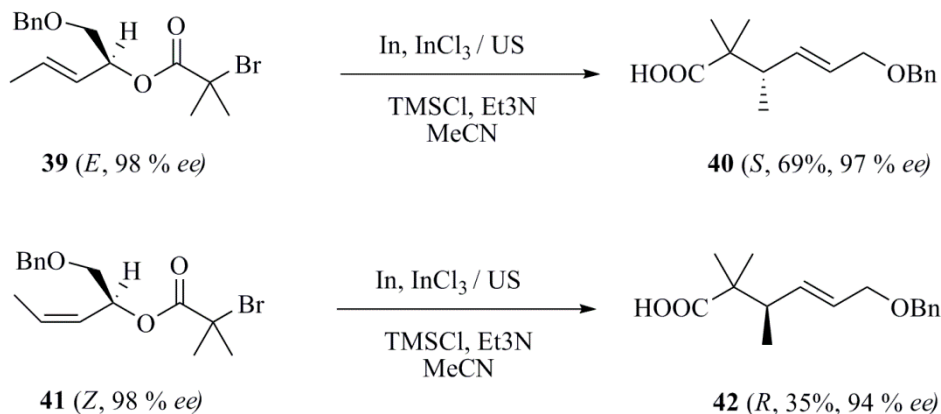
Certainly indium shows an ionization potential comparable to that of electropositive metals, and enables a broad compatibility with numerous functional groups and, unlike alkaline or alkaline-earth elements, has the advantage of performing reactions in an aqueous environment [38,39]. In past development involving Barbier allylation reactions, the allylindation of 1*H*-indole-3-carboxaldehyde with azoles (pyrazole and imidazole compounds) was conducted in aqueous media under sonication. Mechanistically, the one-step protocol involves dehydration and nucleophilic addition leading to a variety of indole derivatives (Scheme 11). Sonication significantly accelerates the overall transformation without affecting reaction yields [40]. The work inspired a multi-component one-pot domino synthesis of convolutamydine A, a natural marine natural product with antinociceptive effects [41], as well as further extension to the preparation of other functionalized indolyl derivatives [42].



Scheme 11. Indole syntheses involving Barbier allylindation promoted by sonication.

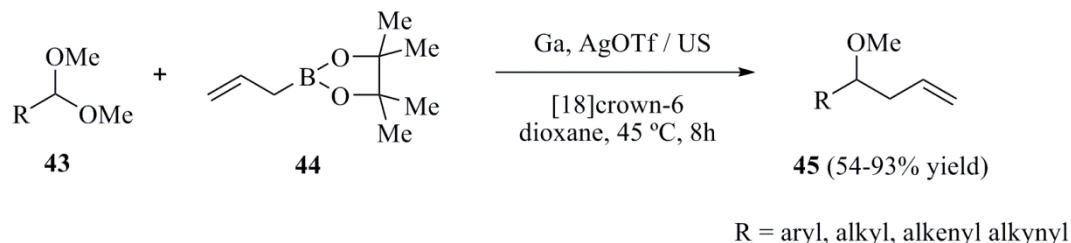
Soengas and associates have also paid attention to the effect of sonication on some indium-promoted reactions, which can be conducted under milder conditions thus preserving high levels of diastereoselection. The group applied the strategy to, for instance, the synthesis of β -lactam carbohydrates [43], β -amino acid and spirodiketopiperazines from sugar lactones [44], or allylation and Reformatsky reactions on oxime ethers [45]. An interesting variation of the classical Reformatsky-Claisen rearrangement has been described by Ishihara et al. The reaction of substituted allyl α -bromoacetates with indium and indium(III) chloride under ultrasound leads to functionalized building blocks bearing quaternary centers [46]. The transformation is run in the presence of a silylating

reagent, and involves presumably the in-situ formation of In(I) species. The protocol offers promising avenues in chiral transfer, as exemplified in the asymmetric reactions shown in Scheme 12 starting from diastereomerically different products. It should be noted that the preparation of univalent indium salts can be successfully accomplished from indium metal employing sonication as well [47].



Scheme 12. Sonochemical Reformatsky-Claisen rearrangement on chiral substrates.

Like indium, lighter metallic gallium has attracted considerable interest in recent years. It is fairly stable under air and moisture and exhibits a low first ionization potential. Moreover, due to its low melting point (ca. 29 °C), it can easily be handled in the liquid phase [48]. Ga(0) has been exploited in a few stoichiometric Barbier reactions [49,50]. The ionic forms show distinctive properties; while Ga(III) is a strong Lewis acid and has been employed in catalytic reactions, the chemistry of Ga(I) is largely underestimated as the low oxidation state tends to undergo disproportionation to Ga(III) and Ga(0). In order to use Ga(0) in catalytic fashion, it should be converted into unstable Ga(I) species. In a recent study, Qin and Schneider described the first catalytic use of elemental gallium through in situ oxidation by Ag(I) and ultrasonic activation [51]. Ga(I)-catalyzed carbon-carbon bond formations involving allyl or allenyl boronic esters and acetals, ketals or amins, proceeded with essentially complete chemo- and regioselectivity in good overall yields (Scheme 13). The reaction time was significantly decreased by switching from conventional heating and stirring (40 °C in dioxane, 24 h) to sonication (40–45 °C, 8 h). The Ga(0)/Ag(I) ratio and the virtual Ga(I) loading were decreased to 2:1 and 5 mol %, respectively, under such conditions without loss of activity. An external ligand [18], crown-6, employed to stabilize Ga(I) catalyst, proved to be critical for full conversion. Remarkably, this reaction could be achieved on a gram scale at low catalyst loading (0.1 mol %).



Scheme 13. Ga(I)-catalysis under sonication for C-C bond formation.

Finely dispersed gallium microspheres with concomitant encapsulation of organic dyes (which include Congo red, crystal violet, phenanthroline, and rhodamine 6G) within them could be achieved by means of ultrasonication in water for a few minutes at 55 °C at a temperature at which Ga is molten. This application, reported by Gedanken and co-workers [52,53], even though disconnected from synthesis, provides potentiality in removing organic pollutants by such microspheres aided by

the mild and relatively inexpensive use of sonication. Scanning electron microscopy (SEM) (Figure 2) and transmission electron microscopy (TEM) images indicated that entrapment of organic molecules takes place in the voids of hollow Ga particles, whereas alternative mechanisms based on adsorption onto the metal surface or interlattice inclusions were ruled out.

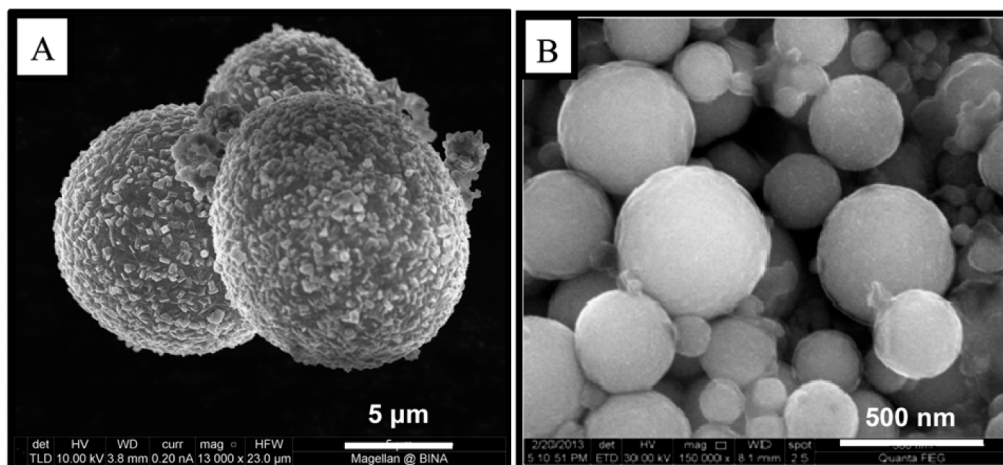


Figure 2. SEM (scanning electron microscopy) images of gallium particles formed after sonication in (A) distilled water and (B) aqueous solution (9.1 mM) of 1,10-phenanthroline. Reproduced with permission from Ref. [53]. Copyright 2014 the Royal Society of Chemistry.

4. Nanostructured Materials from Transition Elements

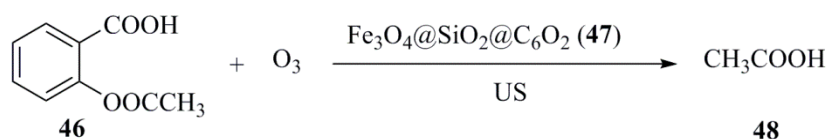
As mentioned above, the application of ultrasound to the preparation of micro- and nanosized materials from inorganic and organic materials represents a fertile field of modern research [8,10,54], and cavitation not only makes their synthesis easier but also induces profound morphological changes that affect the reactivity against other molecules. Although zero-valent elements can be employed, sonochemical procedures often harness the facile formation of metal ion species in solution to induce surface modifications and formation of supported catalysts with high activity. The following examples include cases involving early, middle, and late transition metals, as well as a few cases of so-called inner transition metals comprising the lanthanide *f*-block.

4.1. First-Row Transition Metal NPs

Rahmani et al. synthesized, under the action of ultrasonic irradiation, Cr/clinoptilolite-ZrO₂ nanocatalyst to investigate the CO₂-enhanced dehydrogenation of ethane [55]. Sonication was carried out by applying a pulse ratio (on:off) of 0.3:0.1 s at an input power of 90 W for 60 min. The samples were thoroughly characterized by means of various physicochemical techniques, and the authors determined that sonication generated metal oxide-NPs with sizes of about 4–8 nm, promoting the distribution of metal particles and strengthening the chromium-support interaction. The best performance at 700 °C for 5 h was attained with the Cr/CLT-Z25(U) nanocatalyst giving 38% ethylene yield.

Iron-based nanomaterials are especially popular in terms of facile preparation from inexpensive precursors. Both synthetic and degradation applications are frequently reported for such NPs, which can be reused and/or recycled, thus contributing to sustainable methodologies. Thus, Dai et al. obtained an ozonation catalyst via chemical precipitation and further calcination, assisted by ultrasonication [56]. The authors prepared magnetic core/shell CeO₂ nanoparticles with a Fe₃O₄ magnetic core, a silica mid-layer, and CeO₂ outer layer (47: Fe₃O₄@SiO₂@CeO₂) for the degradation of aspirin (acetylsalicylic acid, ASA, 46) which could also enhance the total organic carbon removal (Scheme 14). The ASA removal with Fe₃O₄@SiO₂@CeO₂ as catalyst conducted for 60 min reached 81.0%, while 67.3% with

$\text{Fe}_3\text{O}_4@\text{SiO}_2$, 66.1% with Fe_3O_4 , and only 64.1% with O_3 alone. This type of catalyst had magnetic recyclability and low metal leaching.

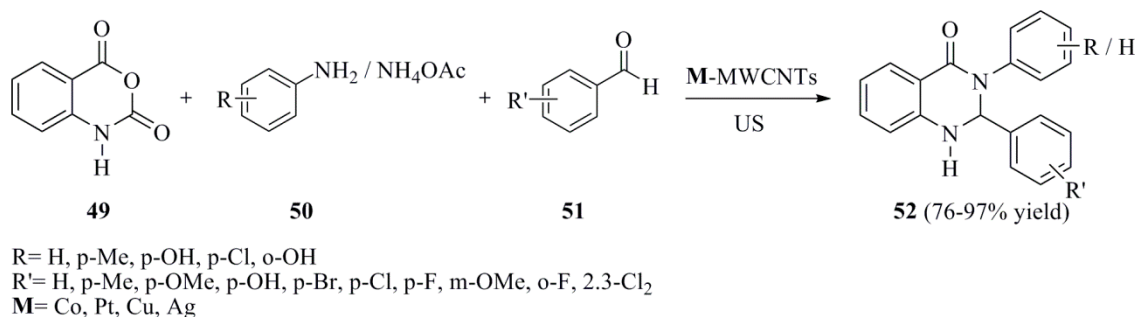


Scheme 14. Degradation of a pharmaceutical compound using an iron-based ozonation catalyst in the presence of ultrasound.

Gobouri et al. have also shown that simultaneous irradiation of Fe_2O_3 -NPs (iron oxide nanoparticles) with light and sonication can enhance their catalytic effects in degradation processes [57]. The catalytic activity was evaluated in the degradation of Eosin Y and Rhodamine B under certain experimental conditions (pH, amount of catalyst, and organic additives). The catalytic efficiency increased significantly, from 53% to 72.5% and 5.59% to 20.79%, respectively, when the degradation was conducted under simultaneous irradiation.

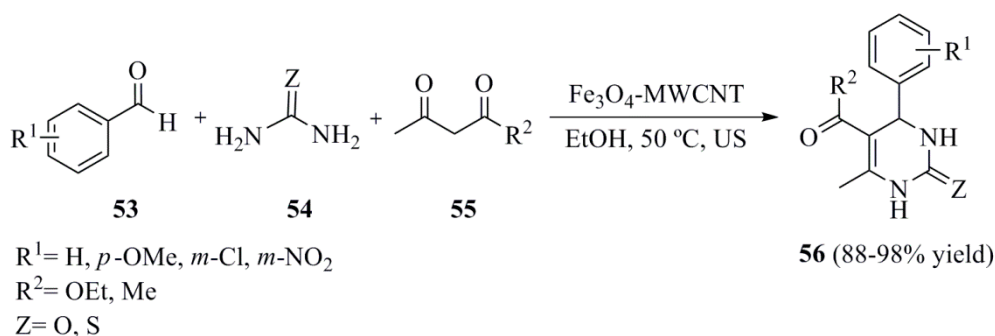
In line with the use of advanced oxidation processes (AOPs) as degradative strategies, a novel method of decomposing ibuprofen (IBP), a widely used anti-inflammatory drug, was developed by Ziylan and Ince [58]. Catalytic ozonation using high-frequency ultrasound and Fe-based species was applied. The optimum concentration of IBP, O_3 flow rate, and US power were $50 \mu\text{M}$, 12 mg min^{-1} , and 0.23 W mL^{-1} , respectively. The most critical parameter was found to be pH, as the latter determined the mass transfer and decomposition of O_3 as well as the diffusion of solutes from the bulk liquid to the interfaces (both gas–liquid and solid–liquid). The maximum degree of oxidation could be obtained with zero-valent iron (ZVI) nanoparticles at pH 3.0 (100%, 58%). The synergy of sonication and ZVI at acid pH was ascribed to a series of factors such as the existence of surface areas enriched with large reaction and nucleation sites, the role of active Fe, reactive oxygen species which promote Fenton-like reactions, and finally the contribution of hydrodynamic shear forces to continuous cleaning of the catalytic surface. The oxidation and mineralization of IBP was efficiently accelerated in 1-h ozonation.

The use of transition metal nanocomposites as catalysts under sonication has also been applied to the synthesis of mono- and disubstituted dihydroquinazolinones (52) in good yields [59]. The reaction depicted in Scheme 15 involves a three-component reaction of isatoic anhydride (49), primary amines or, alternatively ammonium acetate (50), with aryl aldehydes (51) catalyzed by some transition metal multi-walled carbon nanotubes (MWCNTs). The activities of these species were found to decrease in the order: Co–MWCNTs > Pt–MWCNTs > Cu–MWCNTs > Ag–MWCNTs. The protocol showed advantages as mild reaction conditions, easy work-up, green character, energy efficiency and reusable catalysts.



Scheme 15. One-pot multicomponent condensation catalyzed by metal multi-walled carbon nanotubes (MWCNTs) under ultrasound irradiation.

A related multicomponent strategy was reported by Safari and Zarnegar leading to an improved preparation of dihydropyrimidin-one/thione derivatives (**56**) starting from aromatic aldehydes (**53**), urea/thiourea (**54**), and β -dicarbonyl compounds (**55**), using Fe_3O_4 -MWCNT as nanocatalyst under ultrasound irradiation [60] (Scheme 16). This Biginelli transformation tolerates numerous functional groups in the reaction partners and proceeds in short times and good yields, due to the high catalytic activity of the NPs. The catalyst was reused without significant losses in performance and was, in addition, easily recovered from the reaction mixture by means of an external magnet).



Scheme 16. Multicomponent synthesis of dihydropyrimidin-ones/thiones using Fe_3O_4 -MWCNT under ultrasonication.

Nickel NPs, in the form of montmorillonite-supported nickel nanoparticles (Ni-MMT) are good catalysts that can be easily generated through an ultrasound-assisted cation exchange impregnation method within ca. 30 min [61]. Montmorillonites, which are phyllosilicates with a lamellar structure, are ideal candidates for developing a low-cost, anti-coke, and anti-sintering support, thus preventing the agglomeration of NiNPs. The catalysts were evaluated in the production of H_2 by the glycerol steam reforming reaction (GSR) with low CO concentration. The effect of Ni contents and calcination temperatures indicated that a mesoporous Ni-MMT catalyst with 20.9% Ni calcinated at $700\text{ }^\circ\text{C}$ showed the highest activity and stability for GSR conducted at $600\text{ }^\circ\text{C}$.

A nanostructured Co_3O_4 catalyst enables the selective oxidation of vanillyl alcohol to vanillin at $75\text{ }^\circ\text{C}$ and ambient pressure with H_2O_2 as the sole oxidant and water as solvent in conjunction with ultrasound (at 19.95 kHz and volume acoustic power = 0.25 W mL^{-1} determined by calorimetry) [62]. Although both yield and selectivity were modest, such figures were higher under ultrasound in only 15 min (compared to 1 h under silent conditions). Moreover, a commercial Co_3O_4 nanopowder (with a surface area do $32\text{ m}^2\text{ g}^{-1}$) was also less efficient under sonication. The results were ascribed to enhanced physical (mass transfer) and chemical (production of OH radicals by sonicating H_2O_2) effects promoted by ultrasound on the catalyst surface.

Noble and coinage transition metal NPs have been extensively used in recent years in view of the numerous organic transformations accomplished with such metals. The use of NPs often provide more efficient and environmentally benign approaches (by reducing metal loadings and wastes) than the corresponding conventional catalysts employed under homogeneous or heterogeneous conditions. As a representative example, CuAAC reactions affording triazoles with high regioselectivity in good yields, have been performed with stable, water-soluble Cu-NPs synthesized by means of a double-hydrophilic block copolymer as template under 10-min sonication. Such Cu-NPs could further be reused three times without any substantial loss of catalytic efficiency [63].

Surface modification of micro-sized TiO_2 using high-intensity ultrasound was reported by Stucchi and co-workers in order to overcome the lack of photocatalyst activity of the semiconductor under visible light [64]. The authors studied the photodegradation of acetone and acetaldehyde (hydrophilic and polar indoor pollutants) in the gas phase, using an LED lamp. The US-assisted synthesis of metallic copper and copper oxides species at the TiO_2 surface employed CuCl_2 as

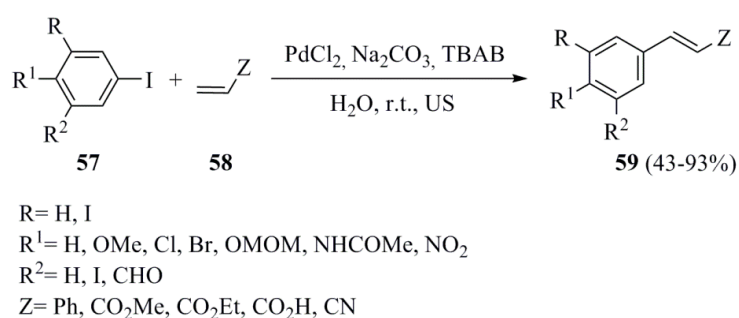
precursor (Cu amounts ranged from 1 to 75 wt %), showing diverse morphologies in accordance with copper content. Ultrasonic parameters (20-kHz frequency, 200 W, and a horn of 13-mm diameter) were important for the preparation of nanoparticles with a good distribution on the TiO₂ support. The optimal ultrasonic operating conditions for the copper deposition (50 W cm⁻², 2.5 h, 62 °C) accelerated the diffusion of solute in the reaction medium, generating available active sites on the TiO₂ surface, thereby increasing the visible light absorption and improving the photocatalytic activity.

4.2. Pd and Pt NPs

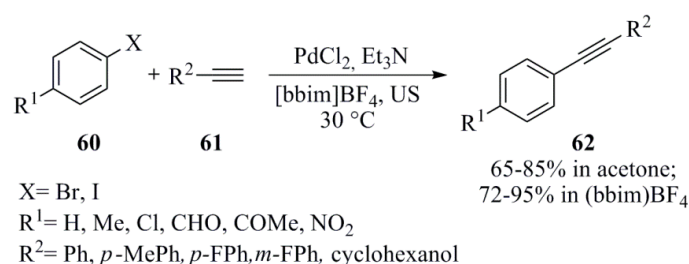
Versatile enough among metal catalysts, palladium has proven its efficiency and broad scope in promoting the quintessential point of organic synthesis, i.e., carbon-carbon bond-forming reactions. Pd-NPs serve as precatalysts, which are produced in situ from Pd salts, usually Pd(II) precursors, then reduced to Pd(0), forming Pd-NPs [65].

Zhang et al. studied an aqueous Heck reaction of halogeno-arenes (**57**) with olefins (**58**) under ultrasonic irradiation at ambient temperature affording the corresponding products (**59**) in moderate to high yields (Scheme 17) [66]. Pd-NPs prepared in-situ were also a recyclable catalyst. Furthermore, the Heck reaction under such benign conditions offered high regioselectivity of para-over ortho-substitution in phenyl iodides (**57**), notably with electron-donating groups. Ultrasound was essential in the formation of Pd-NPs; without it, slow generation and no aggregation of the nanomaterial took place. The insertion of palladium into the C-I bond benefits from the combined action between the surface energy of Pd-NPs and the energy derived from ultrasonic cavitation.

A related coupling, the so-called Sonogashira reaction, which enables the preparation of disubstituted acetylenes (**62**; Scheme 18), has also been conducted with nanoparticulated catalysts and ultrasonic activation by Gholap and associates [67]. The protocol could be performed in short reaction times with high chemoselectivity and good yields at room temperature, under sonication. Comparative analyses were obtained from reactions conducted in acetone and in an ionic liquid, in the absence of a phosphine ligand and co-catalysts. It was determined that ultrasonic irradiation not only generated the Pd(0)-NPs as the active catalyst, but also enhanced the catalytic activity of this species in the cross-coupling reaction.



Scheme 17. Sonochemical Heck reaction with PdNPs in aqueous medium.

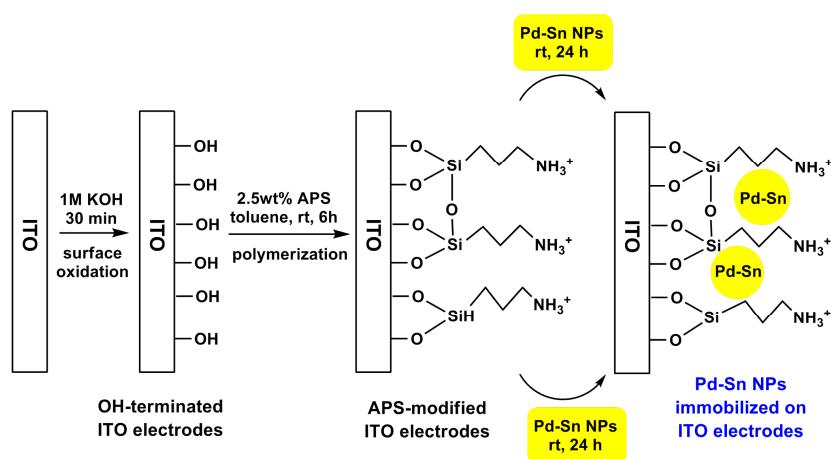


Scheme 18. Sonochemical Sonogashira coupling with in situ PdNPs.

Palladium NPs merged with different supports have also found a variety of applications. The electrochemical performance of Pd-NPs deposited onto carbon-coated LiFePO_4 (LiFePO_4/C) surfaces have been investigated recently [68]. Both Pd-NPs and deposition onto the support were obtained by sonochemical procedure and stirring (at a frequency of 200 kHz and 8.4 W). The structural, morphological and electrochemical performances were evaluated by means of TEM, X-ray diffraction (XRD), and charge–discharge measurements. The size of NPs (homogenous size distributions) on the surface of LiFePO_4/C were tested using various concentrations of Pd(II). It is worth pointing out that the technique can be used to ameliorate the electrochemical performance of LiFePO_4 for battery applications.

Heterometallic NPs can also be prepared by similar strategies of stabilization and deposition, which are enhanced by ultrasonic irradiation, such as the sonochemical reduction of Pd and Au salts to the zero-valent oxidation state followed by immobilization of the resulting nanoparticles on TiO_2 surfaces [69]. The sonolytic oxidation of paracetamol in aqueous solution catalyzed by Pd– TiO_2 and Pd/Au– TiO_2 was especially effective due to their considerably smaller size (than that of Au– TiO_2). Furthermore, the activity of the Pd– TiO_2 nanocomposite was improved under ultrasonic and UV irradiation at 254 nm.

Kim et al. prepared Pd-Sn NPs under ultrasonic irradiation at 20 kHz with an input power of 42 W/cm^2 for 2 h [70]. The electrocatalytic activity for oxygen reduction was evaluated in 0.5 M KOH and was found to be greater than those of Pt or Pd NPs in alkaline media. Pd was present chiefly in the metallic state in the Pd-Sn NPs (with average size of 3–5 nm). The factors that affected the particle size and dispersion of Pd-Sn NPs and, therefore controlled the electroactivity for oxygen reduction were the molar ratio of Pd to Sn ions in solution, their initial concentrations, the volume of ethanol (thereby increasing hydrogen radicals during sonolysis), as well as the amount of citric acid (acting as a stabilizer and controlling the surface properties). In order to assess the electrocatalytic action, indium-doped tin oxide (ITO) electrodes were modified with Pd or Pd-Sn NPs, which involve the initial oxidation of the electrode to make it OH-terminated, followed by aminosilanization with 3-aminopropyl-triethoxysilane (APS) and subsequent polymerization at 100°C . The resulting APS-modified ITO electrode was immersed in a citrate solution of Pd-Sn NPs (Scheme 19).



Scheme 19. In-doped tin oxide (ITO) electrodes modified with Pd-Sn NPs, obtained by sonochemical reduction. Reproduced with permission from Ref. [70]. Copyright 2009 Elsevier Ltd.

A simple process to synthesize C_{60} -Pd polymer spherical nanoparticles (20–200 nm in diameter) was reported by Brancewicz et al. [71]. The polymer was obtained from a benzene solution containing precursors such as the well-known complex of zero-valent palladium ($\text{Pd}_2(\text{dba})_3\cdot\text{CHCl}_3$) and fullerene (C_{60}), and showed a tendency to precipitate in large cubic particles (20–80 μm) which are composed of small spherical nanoparticles (20–200 nm). The procedure takes advantage of the ultrasound energy

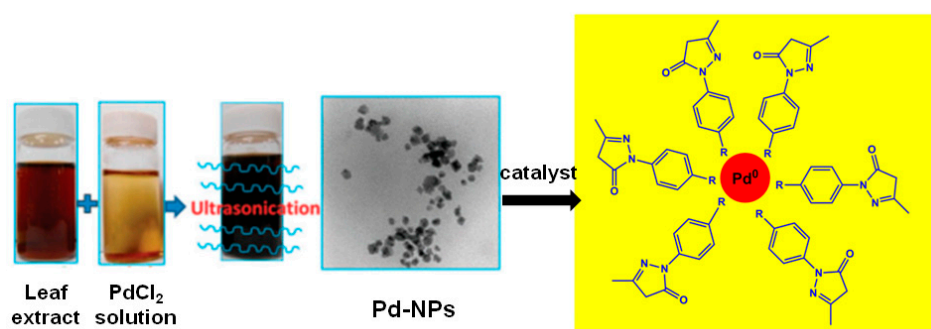
effect to disintegrate the cubic particles in spherical nanoparticles. Moreover, the size of such C₆₀-Pd NPs can be fine-tuned by the concentration of the parent solution, time of polymerization, temperature, and stirring conditions. A solution containing a 3:1 ratio of [Pd] to [C₆₀] led to the most homogeneous size of NPs. Dispersed C₆₀-Pd NPs are stable in many organic protic and aprotic solvents. The thin solid films formed from chemically synthesized nanoparticles exhibited reversible electrochemical properties, e.g., high efficiency of electro-reduction and good capacitance.

Highly homogeneous, spherical porous Pd nanostructures (SPPNs) with rough surfaces were obtained through a facile and rapid ultrasound-promoted reduction [72]. Sonication plays the dual role of speeding up the spontaneous assembly of Pd-NPs to avoid oriented attachment and maintaining a homogeneous dispersion of such nanostructures. The synthesis involves the sonication of an aqueous solution of K₂PdCl₄ plus ascorbic acid for 7 min at 40 °C without any additives or templates. Isolated structures with a narrow size distribution and diameters ranging from 40 to 100 nm (controllable through the concentration of the Pd salt) were obtained. Typical products are formed by loosely packed grains of 2–3 nm with a diameter of 52 nm. The electro-oxidation of formic acid was employed to assess the catalytic performance of the SPPNs. Long-term stability and recyclability makes this nanomaterial a suitable anode catalyst for formic acid-based fuel cells.

Likewise, the ultrasonically assisted synthesis of Pd-Cu nanocatalysts with various Pd loadings and their activities toward CO oxidation has also been reported [73]. The results of catalytic tests indicated that NPs containing a high amount of Pd showed a better catalytic performance at lower temperatures. A nanomaterial of composition Pd(1.5%)-Cu(20%)/Al₂O₃ exhibited the best activity after 95 min of ultrasonic irradiation exposure.

Colmenares et al. developed an outstanding photodeposition method combined with ultrasonic irradiation, i.e., sonophotodeposition (SPD) method [74,75], for preparing bimetallic Pd-Au alloy NPs supported on titania (Pd-Au/TiO₂ P90) [76]. The preparation was accomplished under mild conditions (ambient temperature and pressure), in short times, and without requiring strong reducing agents. The bimetallic system exhibited remarkable catalytic activity (83%), selectivity (70%), and stability in the oxidation of methanol to yield methyl formate. The enhanced catalytic activity was rationalized in terms of synergistic effects by combining Au- and Pd-NPs, and the strong interaction of Pd-Au with titania.

Pd NPs (with sizes between 10 and 17 nm) have also been prepared by a sustainable method that involves the use of a bioreductant, namely an aqueous extract of *Perilla frutescens* leaf, under sonication (ultrasonic bath for 2 h at 60 °C) without any additional surfactant or capping agent [77]. It is thought that polyphenols and flavonoids present in the bio-organic extract reduced Pd(II) to Pd(0). The NPs were then applied to a high-yielding (81%–95%), three-component synthesis of aryl-substituted pyrazolylphosphonates from the corresponding pyrazolones, aryl aldehydes, and triethylphosphite in ethanol (Scheme 20).



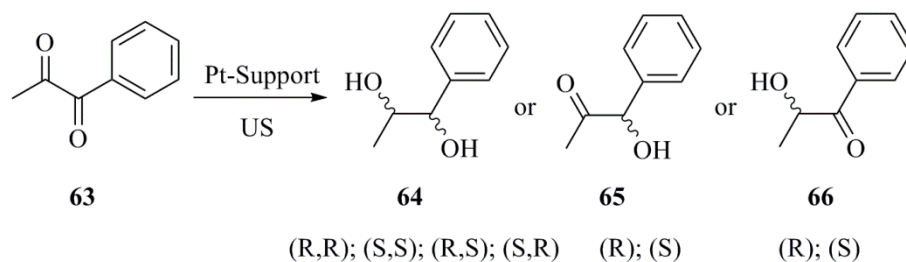
Scheme 20. Ultrasonic generation of PdNPs using bioreduction with *P. frutescens* and subsequent multicomponent synthesis of pyrazolone derivatives. Reproduced with permission from Ref. [77]. Copyright 2015 the Royal Society of Chemistry.

Together with Pd, the heavier congener Pt can be obtained as nanostructured material, stabilized by different ligands and additives under sonication. Pt-NPs have met a myriad of catalytic functions in basic and applied research, some largely related to photocatalysis and electrochemistry. Thus, from 2006 onwards, Colmenares et al. have been working with some titania-based catalysts doped with different transition metals, obtained by the sol-gel method using titanium tetraisopropoxide as precursor [78]. Magnetic stirring (MS) or ultrasound (US) were used to produce the aging of the gel. Sonication enabled the synthesis of pure anatase nanoparticles with increased surface areas, which influence the photocatalytic performance. Further pursuits included not only titanium tetra-isopropoxide, but also titanium tetrachloride as titanium precursor, employing MS, US, microwave (MW), and reflux methodologies for the sol-gel aging procedure [79]. The synthetic protocol was optimized and applied to the generation, by coprecipitation, of a Pt-doped TiO₂ system that was evaluated against the selective photooxidation of propan-2-ol in the gas phase.

The same research group also reported the complete degradation of 3-chloropyridine under the action of photocatalysts based on titania. This reaction was practically completed after 480 min of irradiation [80]. The synthesis of TiO₂-based catalysts was performed using titanium tetra-isopropoxide and acetyl acetonates derived from different metals. The catalysts were obtained by aging the gel under US, MW and heating at reflux. The best solid in terms of material properties—100% anatase NPs, high crystallinity, and high surface area—was obtained under ultrasonic irradiation. Otherwise, the modification of TiO₂ with metals (Fe, Pt, Pd) was unfavorable for photocatalysis. The team also used titanium isopropoxide or titanium tetrachloride as precursors of TiO₂-based catalysts, for the selective photo-conversion of 2-butenol to 2-butenal in the liquid phase, as well as gas-phase photo-oxidation of 2-propanol to acetone [81].

Vinodgopal et al. employed an ultrasound dual frequency arrangement at 20 kHz (ultrasound horn-type transducer) and 211 kHz (high-frequency transducer) operating in tandem to obtain bi- and single layered graphene with Pt-NPs dispersed on that 2D-material [82]. These hybrid composites showed good electrocatalytic activity in the oxidation of methanol. The dual frequency arrangement enabled the reduction of the graphene oxide sheets while ensuring a high level of exfoliation. The latter issue is critical as optimal properties of graphene largely depend on its thickness; ultrasound being a common energy source to achieve successfully liquid-phase exfoliation [83,84].

The enantioselective hydrogenation of 1-phenyl-1,2-propanedione (**63**) was performed by different Pt-modified catalysts: Pt/Al₂O₃, Pt/SiO₂, Pt/SF (silica fiber), and Pt/C catalysts, also decorated with cinchonidine in a pressurized reactor subjected to ultrasonic irradiation (Scheme 21) [85]. The initial rate along with regio- and enantioselection trends were interrogated for different pretreatments, solvents, and US powers. Sonication improved significantly both enantioselection and activity of the Pt/SF catalyst. On using 5 wt % Pt/SF, pronounced enhancements of the initial rate, enantio- and regioselectivity could be observed under sonication relative to silent experiments. In solvents of high vapor pressure (e.g., methyl acetate) ultrasound had negligible effects on both reaction rate and product selection, while solvents exhibiting low vapor pressures (mesitylene in particular) resulted in the highest ultrasound-induced enhancements. From a chemical viewpoint, this asymmetric reduction is a complex process giving rise to four isomeric hydroxyketones (**65** and **66**), which can undergo further hydrogenation to the corresponding diols (**64** as diastereomeric mixture). The authors only assessed the first hydrogenation step, measuring discrete enantiomeric excesses (47% *ee* at 50% conversion and up to 60% *ee* at 98% conversion). The effects caused by ultrasound were dependent on the catalyst and its pretreatment. The enhancement of *ee* under sonication was only noticeable with Pt/SF (34% *ee* versus 17% *ee* under silent conditions at 50% conversion). This was attributed to a substantial modification of metal particle size distribution (as viewed by SEM) under acoustic irradiation.



Scheme 21. Stereoselective hydrogenation of 1-phenyl-1,2-propanedione improved by sonication.

Highly dispersed Pt-NPs could also be incorporated into CeO₂ nanopowders through a one-step ultrasound-promoted reduction [86]. The efficiency of the resulting Pt/CeO₂ catalysts was tested in the combustion reaction of ethyl acetate. Total conversion could be achieved at low temperature. It should be noted that the sonochemical preparation of the catalyst led to Pt-NPs with diameters of 2–4 nm and favored the homogeneous intercalation into CeO₂ nanopowders.

Selvaraj et al. reported the preparation of a new supporting material formed by polythiophene (PTh) and multiwalled carbon nanotubes (MWCNTs) (i.e., PTh-CNTs), which could be obtained through in situ polymerization of thiophene on carbon nanotubes using FeCl₃ as oxidant under ultrasound [87]. Such polythiophene/CNT composites were further doped with Pt- and Pt-Ru NPs by reduction of the corresponding metal salts with formaldehyde as reducing agent at pH 11. The resulting Pt/PTh-CNT and Pt-Ru/PTh-CNT materials were tested in the electrocatalytic oxidation of ethylene glycol, finding that the bimetallic catalyst, Pt-Ru/PTh-CNT showed a prolonged stability and better storage characteristics than Pt/PTh-CNT.

Nanoparticles made of Pt₃Co with Pt-enriched shells on a carbonaceous support have been generated by a one-step ultrasonic polyol procedure from Pt(acac)₂ (acac = acetyl acetonate) and Co(acac)₂ as metal precursors [88]. Sonication promoted the transformation of Co(acac)₂ and delayed the conversion of Pt(acac)₂ into nanoparticles; an observation consistent with the different vapor pressures of Pt(II) and Co(II) acetyl acetonates. This sonochemical variation afforded Pt-NPs that were superior electrocatalysts for oxygen reduction than other commercially available catalysts like Pt/C. Likewise, Jiang et al. investigated the coverage of Pt atoms on PtCo-NPs and their catalytic effect on oxygen reduction [89]. PtCo-NPs having different coverages of Pt atoms were synthesized according to various methods, which included microemulsion synthesis and ultrasound-assisted microemulsion, the latter being especially efficient and yielding the most active catalyst (ascribed to an increase of active surface coatings of Pt atoms on NPs). The rate of oxygen reduction catalyzed by such ultrasound-generated PtCo-NPs was approximately four times higher than that of the PtCo catalyst obtained through a conventional method, and they could catalyze the oxygen reduction to water without detection of H₂O₂ as intermediate product.

Nagao et al. evaluated the effect of sonication during the impregnation of bimetallic Pt-Ru-NPs on a carbonaceous support (ultrasonically dispersed) by the reduction of Pt and Ru ions with NaBH₄ [90]. The catalysts prepared under sonication were single-nanometer-sized particles, while Pt-Ru particles with significant aggregation were instead detected in the conventional, non-irradiated sample. In addition, the former catalyst was much more efficient for methanol oxidation than Pt-Ru-NPs generated under silent conditions. The enhanced effect of ultrasound on the catalytic activity was also established at concentrations of Pt, Ru, and carbonaceous support as high as 3.0 mM, 1.2 mM, and 1065 mg L⁻¹, respectively. In other words, ultrasonically-activated NPs remained unaffected in catalytic activity as the concentrations of metal ions and carbon increased.

In a related study, series of Ag-, Pt-, and Pt/Ag-NPs supported on carbon substrates as electrocatalysts were generated under ultrasonic irradiation without consecutive thermal treatments [91]. Bimetallic-NPs were sphere-shaped agglomerates with a higher particle size than the corresponding single-metal species, which were less than 10 nm in diameter. The Pt-Ag/C system showed significant

enhancement of electrochemical activity (oxygen reduction), 1.5 times higher, with respect to a Pt/C catalyst from commercial suppliers.

4.3. Ag and Au NPs

The preparations of silver and gold NPs have been widely documented in recent years and this trend will continue for years to come in view of their high versatility. Sonication has obviously added to the repertoire of methods employed in synthesis. Ag-NPs, currently obtained by different green routes [92], exhibit a remarkable antibacterial activity, whose mechanism of action has been investigated in detail as well [93]. Thus, Manjamadha and Muthukumar synthesized Ag-NPs in only 10 min using an aqueous extract of *Lantana camara* L. as bioreductant and capping reagent under ultrasound [94]. Both TEM (Figure 3) and Fourier transform infrared spectroscopy (FTIR) studies confirmed that the weed plant played a key role in the bioreduction and stabilization of NPs by electrostatic interaction of OH groups present in the polyphenols and amide linkages of the protein. Finally, the antioxidant activity exerted by such Ag-NPs was checked using the 2,2-diphenyl-1-picrylhydrazyl (DPPH) test. Moreover, the synthesized Ag-NPs had remarkable antibacterial activity versus both Gram positive and Gram negative specimens.

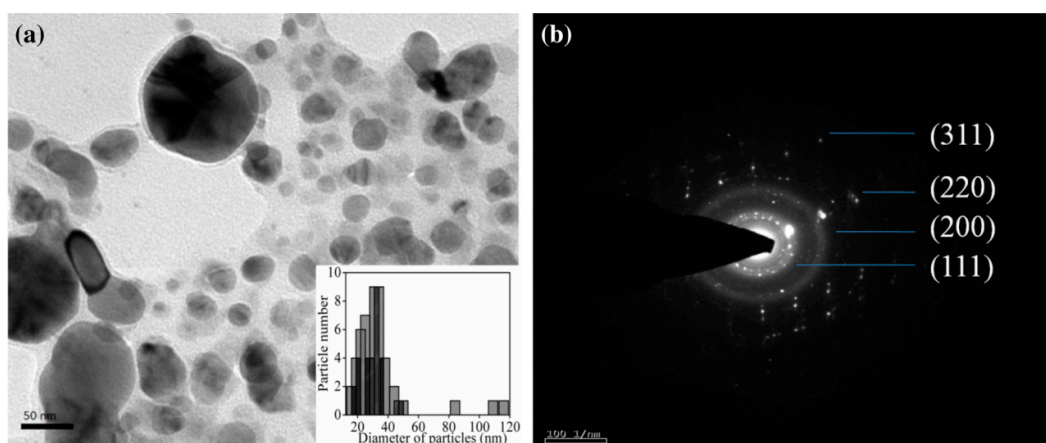


Figure 3. (a) TEM (transmission electron microscopy) images of Ag-NPs generated from *Lantana camara* L. extract under ultrasound. The box shows the resulting particle size distribution; (b) SAED (selected area electron diffraction analysis) pattern. Reproduced with permission from Ref. [94]. Copyright 2016 Springer.

Highly ordered TiO₂ nanotube arrays loaded with Ag-NPs were synthesized at low AgNO₃ concentrations using a common UV lamp through ultrasound-aided photochemistry [95]. It was shown that the concentration of Ag-NPs deposited on TiO₂ nanotubes was sufficient to considerably improve the photoelectrical and photocatalytic activities of the TiO₂ nanotube array. Compared with pure TiO₂, Ag-doped TiO₂ nanotubes generated from 0.006 M AgNO₃ through the hybrid US-assisted photochemical methods had higher photocatalytic degradation rate (3.7 times) and higher photocurrent (1.2 times). The enhanced photocatalytic behavior of the Ag-TiO₂ system was assessed through the elimination of methylene blue (MB) dye in aqueous solution (at an initial concentration of 8 mg L⁻¹). A 200-W high pressure Hg lamp with an emission wavelength of 365 nm was employed as UV-light source, while the changes in MB concentration were obtained by measuring the absorbance intensity at 660 nm. Other authors have also synthesized Ag/TiO₂ composite NPs in ethylene glycol in basic medium (NaOH) through a sonochemical process [96].

A new and stable nanostructured catalyst with high activity towards oxygen electro-reduction in acid electrolytes was introduced by Pech-Pech and co-workers [97,98]. The authors reported the preparation of Ag-rich NPs within a PtPd-enriched area (Ag@Pt_{0.1}Pd_{0.1}). The catalyst was synthesized

in a one-pot protocol by applying intense ultrasound, reducing Ag, and then Pt and Pd salts with NaBH_4 in the presence of trisodium citrate, and finally adding XC-72 (a multi-purpose conductive carbon black). Structural characterization of the resulting catalysts revealed that the amount of Pt and Pd in the shell had a pronounced effect on electro-reduction. The optimal activity was obtained for a catalyst of composition $\text{Ag@Pt}_{0.3}\text{Pd}_{0.3}/\text{C}$, which was a useful alternative to Pt/C .

Nanostructured silver vanadates with nano-rod shape (diameter of 50–200 nm and length of 0.5–2.0 μm) could be obtained by means of hydrothermal treatment assisted by US and MW techniques [99]. Silver vanadates showed a strong absorbance in the UV–vis zone at 470–500 nm and had much higher photocatalytic efficiency in the decomposition of MB under visible light exposure compared to common TiO_2 NPs. Notably, such Ag vanadates also exhibited antibacterial activity, thus adding extra value to potential applications in environmental remediation.

An easy and efficient technique for the synthesis of Ag-NP colloids with cherry- or raspberry-type morphologies was reported by Lei et al. [100]. The approach involves the self-assembly of a copolymer to micelles, which served as a compartment for the generation of NPs with the assistance of ultrasound. The above-mentioned morphologies depended on the amount of AgNO_3 loading, the nature of the reducing agent and external conditions. Sonication favored the diffusion of AgNO_3 and polyethyleneimine (PEI) affording nucleation sites that were well distributed through the micellar cores and led to cherry-like Ag-NP colloids. Moreover, PEI is a nontoxic reducing agent with a slow reaction rate capable of controlling both nucleation and growth processes. Likewise, it serves as protective agent for the resulting Ag-NPs.

Saha et al. described an ultrasound-assisted green procedure for the synthesis of carbohydrate polymer-inspired Ag-NPs using tyrosine and starch, both being naturally-occurring substances [101]. Starch-stabilized Ag-NPs were prepared in water using a small amount of tyrosine as a non-harmful reducing agent. The cytotoxicity of the resulting Ag-NPs on the peritoneal macrophages of Wistar rat was evaluated and confirmed a higher selectivity to filaricidal and larvicidal activity (Figure 4) than that of commercially available ones.

The sonogeneration and catalytic effect of Au-NPs is well documented in recent literature. Kuo et al. synthesized Au-NPs coated on TiO_2 (ranging from 2 to 80 nm in diameter) by varying the pH values from 3 to 7, based on sonoelectrochemical reductions for 3 h [102]. Acetaldehyde solutions in ethanol were almost completely degraded (ca. 95%) based on Au-NPs having the smallest mean diameter of 2 nm. The catalytic activity for acetaldehyde decomposition was markedly reduced in the presence of Au-NPs of greater diameters. Moreover, the optimal sizes of Au-NPs on TiO_2 to produce the strongest surface-enhanced Raman scattering (SERS) effects were ca. 60 nm, under a 785-nm irradiation for probe molecules of Rhodamine 6G and polypyrrole.

In line with the above-mentioned applications, a 2011 review by Wen et al. detailed the use of supported noble metal NPs (Au/TiO_2 , Au/ZrO_2 , Ag/AgCl) as efficient catalysts for selective chemical syntheses and degradation of environmental pollutants [103]. Thus, the NPs could effectively catalyze solar-energy conversion into chemical energy (i.e., oxidation of alcohols, thiols, and benzene into carbonyls, disulfides, and phenol, respectively, or the reduction of nitro-aromatic compounds to the corresponding azo derivatives). Under ultrasound irradiation, the supported NPs could also catalyze the generation of hydrogen from water. Furthermore, a variety of contaminants (bearing different functional groups: aldehyde, alcohol, carboxylic acid, phenolic compounds, and organic dyes) were significantly decomposed, and completely degraded under the action of ultrasound.

Two catalysts containing $\text{Au}/\text{TiO}_2/\text{C}$ were produced by means of US and MW irradiations by George et al. [104]. The deposition of Au colloids onto powdered TiO_2/C , was performed by means of a solvated metal atom impregnation (SMAI) method, which provided highly-dispersed Au particles without requiring high-temperature calcination and reduction steps, which often lead to particle sintering. The catalytic performance of 1 wt % $\text{Au}-\text{TiO}_2/\text{C}$ -based catalysts, both sonochemically and microwave irradiated was evaluated for the oxidation of CO in the range of 0–300 $^\circ\text{C}$ and compared to that of a commercial catalyst containing 1 wt % $\text{Au}-\text{TiO}_2$ (Degussa-P25). Figure 5 shows the

different patterns of the above-mentioned catalysts viewed by transmission electron microscopy (TEM). An increase in CO conversion was observed for the ultrasonically-derived catalyst at low temperature. Furthermore, the reactivity observed for this oxidation followed the order Au/TiO₂/C (US) > Au/TiO₂ (P25) > Au/TiO₂/C (MW).

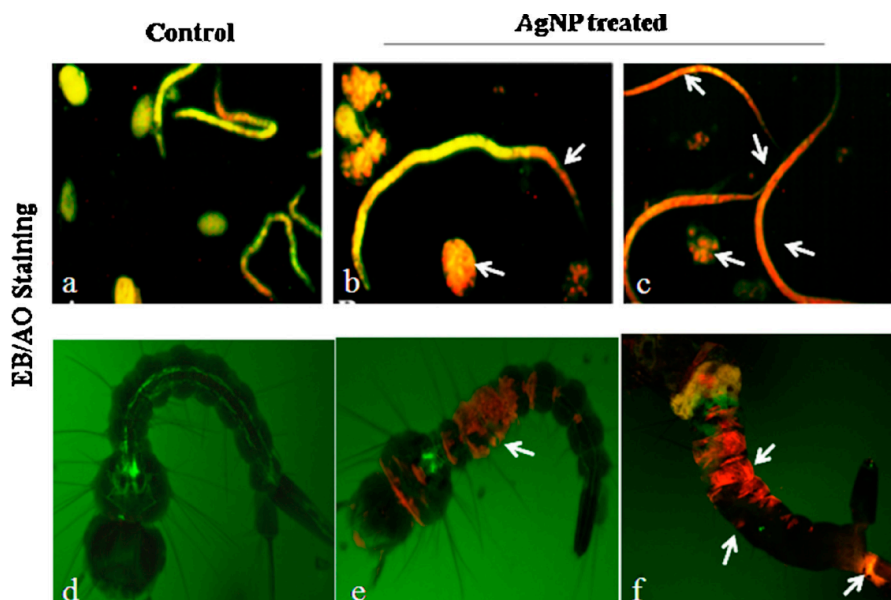


Figure 4. Ethidium bromide (EB)/acridine orange (AO) stained oocyte, microfilaria of *S. cervi* and larvae of *C. quinquefasciatus*. (a) Control, (b) parasites treated with 8.85 µg/mL of Ag-NP10, (c) parasites treated with 28.3 µg/mL of Ag-NP10, (d) control, (e) larvae treated with 21.95 µg/mL of Ag-NP10, and (f) larvae treated with 117.1 µg/mL of Ag-NP10. Reproduced with permission from Ref. [101]. Copyright 2015 Elsevier Ltd.

Sonochemically prepared Au, Pt and Pd NPs could be successfully immobilized onto TiO₂ after prolonged sonication [105]. Sonochemically-generated catalysts showed higher activities than those prepared by conventional protocols as evaluated in the production of hydrogen from ethanol-containing aqueous solutions. The reactivity was markedly dependent on the type of metal NPs and their dimensions. Small Pt-NPs did effectively restrict side reactions arising from recombination of electrons and holes and released hydrogen at a higher rate.

Core-shell nanostructures consisting of Au-NPs within shells of Ag NPs-filled polymer (Au-core/Ag-PVP-shell) were synthesized by Kan and co-workers in a two-step sonication-assisted reduction procedure [106]. Ag-NPs acted as reductive agent for Au(III) ions in the presence of poly(vinylpyrrolidone) (PVP). After sonication, solidification and spherulite growth of the polymer chain was induced on the as-formed Au-NPs, such that tiny Ag-NPs were embedded in the crystalline matrix of polymer spherulites. The formation of core-shell NPs was dependent on the redox potentials of ions in solution, the coordinating ability of such ionic species to stabilize PVP, as well as the crystalline and interlinkage degrees of such a polymer during ultrasonic irradiation. An ultrasonic cleaner, working at 40 kHz with an output power of 360 W, was sufficient to produce the Au/Ag composite in the absence of oxygen. The stabilizing role of polymers and surfactants in nanoparticle production has likewise been highlighted by Park et al., who synthesized colloidal, uniformly dispersed hybrid nanocomposites constituted by polypyrrole (PPy) and Au-NPs (or Pt-NPs) [107]. The procedure, assisted by ultrasonic irradiation, involved reduction of Au(III) ions and pyrrole monomer oxidation in an aqueous solution containing sodium dodecyl sulfate (SDS).

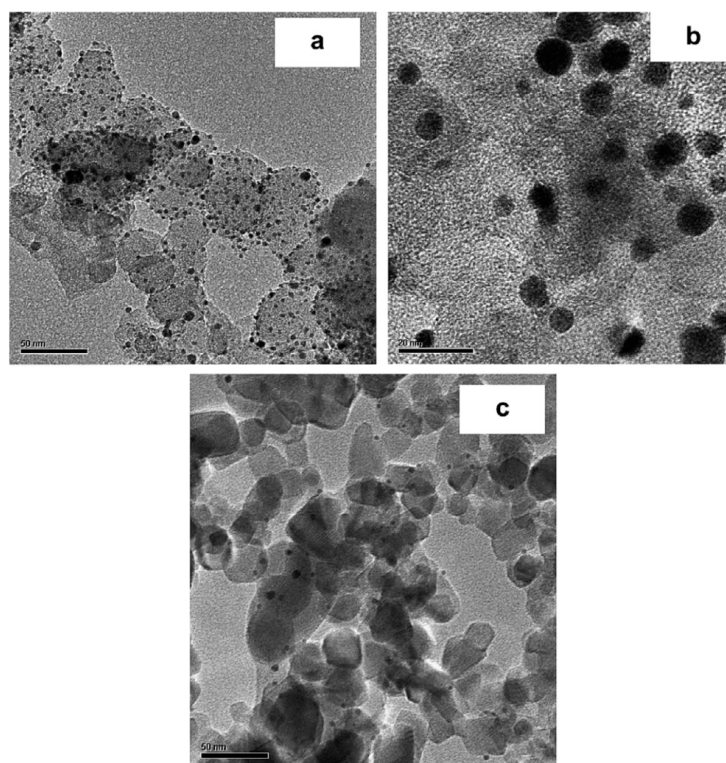


Figure 5. TEM images of (a) 1% Au-TiO₂ (anatase)/C (under US), where black dots are Au-NPs; (b) 1% Au/TiO₂ (anatase)/C (under MW), and (c) 1% Au/TiO₂-P-25, the last support coming from Degussa. Reproduced with permission from Ref. [104]. Copyright 2007 Elsevier B.V.

The construction of a highly efficient anode catalyst for oxygen evolution reaction (OER) was reported in 2015 and consisted of a combination of multiwalled carbon nanotubes, metallic Au, and transition metal-oxide (i.e., CNTs-Au@Co₃O₄) generated under high-intensity ultrasound [108]. The tubular architecture provides enough active centers for OER and enables fast mass and charge transports. The Co₃O₄ layer protects Au-NPs against further detachment, and reciprocally Au facilitated the production of Co(IV) species for OER due to its greater electronegativity.

It should be finally pointed out that Au-NPs can be efficiently generated by means of high-intensity focused ultrasound (HIFU), working at 463 kHz [109]. Formation of NPs proceeds through the reduction of Au(III) ions to Au(0) by radicals generated under ultrasonic cavitation. TEM images revealed that NPs exhibit irregular shapes at low power (30 W), mainly icosahedral at 50 W, and finally nanorods at 70 W. The size decreased with a narrower size distribution as the acoustic power increased.

4.4. Lanthanide NPs

Vilela and co-workers prepared highly crystalline lanthanide composite materials [Ln(Hpmd)(H₂O)], where Ln³⁺ can be Eu³⁺, Gd³⁺, or Tb³⁺ ions, and the organic linker is 1,4-phenylenebis(methylene)diphosphonic acid (H₄pmd) as building block [110]. The authors used three different strategies based on heating procedures of the reaction containers, including classical hydrothermal synthesis (180 °C for 3 days), MW-assisted heating (50-W power at 40 °C for 5 s), and US-promoted synthesis which allowed, for highly diluted mixtures (Ln³⁺:H₄pmd:H₂O ratio = 1:1:7200), the generation of isolated nano-crystals at room temperature within 5 min of acoustic irradiation. The Eu-containing compound was evaluated in the methanolysis of styrene oxide conducted at 55 °C showing diverse catalytic activity and selectivity. Using the ultrasonic procedure it was feasible to significantly reduce both the temperature (from 180 °C to room temperature) and reaction times (from 3 days to 5 s), without affecting phase purity and crystallinity.

In a recent and very detailed study on rare earth-doped nanopowders, $\text{ZrO}_2:\text{Dy}^{3+}$ NPs were obtained by sonication (ultrasonic horn at 20 kHz, 300 W at 333 K) in the presence of cetyltrimethylammonium bromide (CTAB) as surfactant [111]. The resulting NPs exhibited different shapes and sizes depending on the irradiation times and the quantity of CTAB as revealed by SEM images. Flower-like morphologies were obtained after prolonged irradiation (up to 6 h) and increased with frequency (from 20 to 24 kHz). This suggests a complex evolution of self-assembly and growth of NPs, dictated to a significant extent by the surrounding surfactant (Figure 6). The nanopowders had excellent luminescent properties that were utilized to reveal latent fingerprints (LFPs) on various surfaces (Figure 7). In addition, the photocatalytic behavior of $\text{ZrO}_2:\text{Dy}^{3+}$ NPs was evaluated in the degradation of methylene blue dye.

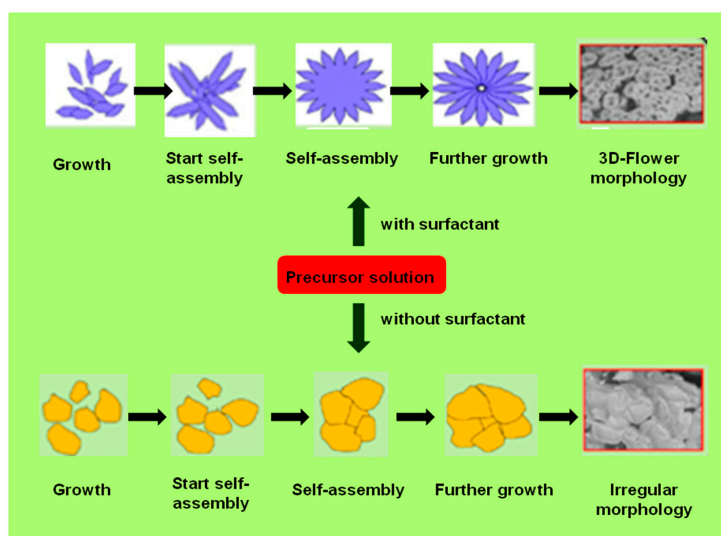


Figure 6. Schematic diagram depicting the formation of $\text{ZrO}_2:\text{Dy}^{3+}$ -NPs (3 mol %) with and without cetyltrimethylammonium bromide (CTAB) and SEM images of the resulting morphologies. Reproduced with permission from Ref. [111]. Copyright 2017 the American Chemical Society.

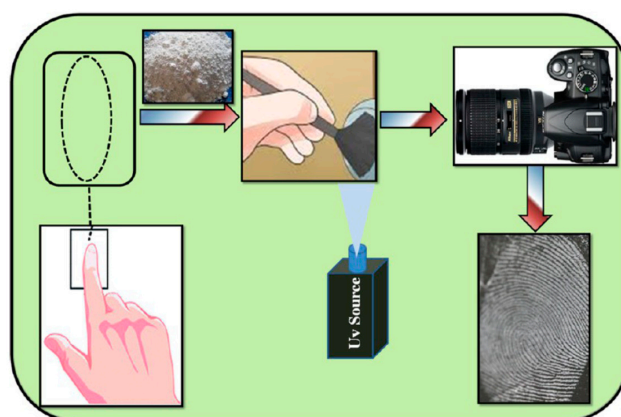


Figure 7. Sequential illustration highlighting the development of latent fingerprint (LFP) detection using $\text{ZrO}_2:\text{Dy}^{3+}$ (3 mol %): (i) impression of fingerprints on different substrates; (ii) applied onto the substrate to stain the fingerprint; (iii) UV light is then used to irradiate the fingerprint to emit white light, and (iv) revealing the fingerprint with high sensitivity and contrast. Reproduced with permission from Ref. [111]. Copyright 2017 the American Chemical Society.

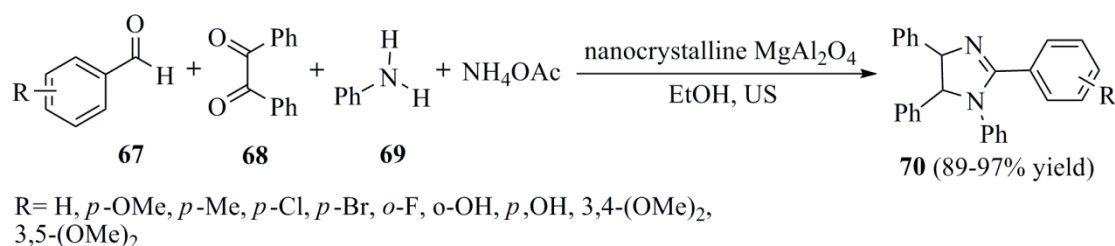
4.5. Main-Group NPs

Aluminum NPs have been isolated and stabilized by reaction, under ultrasonication, of SiCl_4 and LiAlH_4 in the presence of poly(vinylpyrrolidone) (PVP) at ambient temperature [112]. The sonochemical procedure (1 h under nitrogen stream) was used to produce spherical Al NPs with reasonably narrow size distribution (2–15 nm), integrated at random positions of the PVP matrix. This transformation also releases H_2 and volatile hydrosilanes as side products. Thermal analysis of such composites unveiled their stability up to 422 °C by gradual oxidation in air.

In another interesting application, Kumar et al. described the production of enantio-selective gallium particles by synthesizing them in aqueous solutions of D- or L-tryptophan, thereby inducing some imprinted chirality in their structure [113]. Chiral imprinting could be achieved by ultrasonic irradiation (for 3 min at 55 °C) of molten Ga covered by an aqueous solution of D- or L-tryptophan, affording a grey suspension of particles, which were centrifuged at 6000 rpm for 10 min. The resulting products are micro- or nano-particles of Ga encapsulating one of the enantiomers. After leaching of the enantiomer in water, molecular scaffolds are left on the surface of the Ga particles, which then enabled the entrapment of the specific enantiomer from the racemate (i.e., DL-tryptophan). Unfortunately, the enantiomeric excesses were poor (from 6% to 12% *ee*) as determined by polarimetry, circular dichroism and chiral HPLC. However, the method appears to be promising enough en route to chiral imprinting mediated by metal or metal ion NPs generated under sonication.

More recently Gedanken and his group, who have significantly advanced the subject of Ga-based materials sonofabrication, reported a one-step procedure that yields Ga-doped carbon-dots on Ga-NPs from polyethylene glycol (PEG 400) and molten gallium [114]. The resulting nanomaterial, Ga@C-dots@Ga-NPs, was deposited on a glass substrate and further evaluated for neural growth. Cells grown on the aforementioned substrate showed a 97% increase in the number of branches resulting. It is noteworthy that the sonochemical protocol (conducted with a US probe at 20 kHz, 70% amplitude, 70 °C for 2.5 h) enabled both facile fabrication and coating. The latter can be attributed to ultrasonic cleaning that prevents metal oxidation by atmospheric oxygen and avoids the concomitant passivation on the C-dot surface.

In a more-oriented synthetic application, Safari et al. reported a convenient synthesis of 1,2,4,5-tetrasubstituted imidazoles (**70**) through a four-component one-step condensation of a substituted aromatic aldehyde (**67**), benzyl (**68**), phenyl amine (**69**), and ammonium acetate with nanocrystalline magnesium aluminate (MgAl_2O_4) in ethanol under ultrasound (Scheme 22) [115]. The protocol shows the typical advantages of sonochemically accelerated reactions in terms of high yields, mild conditions, short reaction times, and easy work-up.



Scheme 22. Ultrasound-promoted synthesis of 1,2,4,5-tetrasubstituted imidazoles mediated by Mg/Al NPs.

5. Conclusions

In this review we have provided some aspects and applications, mainly gathered in the last decade, of metals and metal ions, either massive or micro/nano-structured form, under the action of an ultrasonic field. The latter constitutes a well-known and established method that rivals and often surpasses the effects of conventional thermal protocols. Along with evident pluses of acceleration,

selectivity, and good overall yields, sonication represents a low-cost strategy, affordable by most laboratories, which can be fine-tuned by simply adjusting empirical parameters such as frequency, input power, or solvents of choice as sound propagation and cavitation implosion are largely influenced by the fluid's properties. In addition, ultrasonic devices can be combined with other irradiation and activation methods, and scaling up can also be easily accomplished. Clearly, one should look forward to developing and improving organic and organometallic reactions in the near future by placing metal derivatives in the vicinity of ultrasound beams.

Acknowledgments: The authors deeply acknowledge Universidad Nacional del Sur (UNS) and Consejo Nacional de Investigaciones Científicas y Técnicas (CONICET), the Junta de Extremadura-FEDER (Grant GR15022), and the University of Turin (Ricerca locale 2015) for financial support.

Author Contributions: All authors contributed equally to the redaction of this review. All authors have given approval to the final version of the manuscript.

Conflicts of Interest: The authors declare no conflict of interest. The founding institutions had no role in the design of the study; in the collection, analyses, or interpretation of data; in the writing of the manuscript, as well as in the decision to publish the results.

References

1. Suslick, K.S.; Doktycz, S.J. Effects of ultrasound on surfaces and solids. In *Advances in Sonochemistry*; Mason, T.J., Ed.; JAI Press Ltd.: London, UK, 1990; Volume 1, pp. 197–230.
2. Pugin, B.; Turner, A.T. Influence of ultrasound on reactions with metals. In *Advances in Sonochemistry*; Mason, T.J., Ed.; JAI Press Ltd.: London, UK, 1990; Volume 1, pp. 81–118.
3. Tomlinson, W.J. Effect of ultrasonically induced cavitation on corrosion. In *Advances in Sonochemistry*; Mason, T.J., Ed.; JAI Press Ltd.: London, UK, 1990; Volume 1, pp. 173–195.
4. Luche, J.-L. Sonochemistry. From experiment to theoretical considerations. In *Advances in Sonochemistry*; Mason, T.J., Ed.; JAI Press Ltd.: London, UK, 1993; Volume 3, pp. 85–124.
5. Cintas, P.; Luche, J.-L. Organometallic sonochemistry. In *Synthetic Organic Sonochemistry*; Luche, J.-L., Ed.; Plenum Press: New York, NY, USA, 1998; Chapter 5; pp. 167–234.
6. Luche, J.-L. Ultrasonically promoted carbonyl addition reactions. In *Advances in Sonochemistry*; Mason, T.J., Ed.; JAI Press Ltd.: London, UK, 1990; Volume 1, pp. 119–171.
7. Cintas, P.; Palmisano, G.; Cravotto, G. Power ultrasound in metal-assisted synthesis: From classical Barbier-like reactions to click chemistry. *Ultrason. Sonochem.* **2011**, *18*, 836–841. [[CrossRef](#)] [[PubMed](#)]
8. Manickam, S.; Kumar Rana, R. Production of nanomaterials using ultrasonic cavitation—A simple, energy efficient and technological approach. In *Ultrasound Technologies for Food and Bioprocessing*; Feng, H., Barbosa-Cánovas, G.V., Weiss, J., Eds.; Springer: Heidelberg, Germany, 2011; Chapter 15; pp. 405–444.
9. Gedanken, A. Doping nanoparticles into polymers and ceramics using ultrasonic irradiation. *Ultrason. Sonochem.* **2007**, *14*, 418–430. [[CrossRef](#)] [[PubMed](#)]
10. Xu, H.; Zeiger, B.W.; Suslick, K.S. Sonochemical synthesis of nanomaterials. *Chem. Soc. Rev.* **2013**, *42*, 2555–2567. [[CrossRef](#)] [[PubMed](#)]
11. Verdan, S.; Burato, G.; Comet, M.; Reinert, L.; Fuzellier, H. Structural changes of metallic surfaces induced by ultrasound. *Ultrason. Sonochem.* **2003**, *10*, 291–295. [[CrossRef](#)]
12. Skorb, E.V.; Möhwald, H.; Irrgang, T.; Fery, A.; Andreeva, D.V. Ultrasound-assisted design of metal nanocomposites. *Chem. Commun.* **2010**, *46*, 7897–7899. [[CrossRef](#)] [[PubMed](#)]
13. Cravotto, G.; Cintas, P. Power ultrasound in organic synthesis: Moving cavitation chemistry from academia to innovative and large-scale applications. *Chem. Soc. Rev.* **2006**, *35*, 180–196. [[CrossRef](#)] [[PubMed](#)]
14. Gedanken, A. Using sonochemistry for the fabrication of nanomaterials. *Ultrason. Sonochem.* **2004**, *11*, 47–55. [[CrossRef](#)] [[PubMed](#)]
15. Gawande, M.B.; Bonifácio, V.D.B.; Luque, R.; Branco, P.S.; Varma, R.S. Solvent-free and catalysts-free chemistry: A benign pathway to sustainability. *ChemSusChem* **2014**, *7*, 24–44. [[CrossRef](#)] [[PubMed](#)]
16. Thirumurugan, P.; Matusiuk, D.; Jozwiak, K. Click chemistry for drug development and diverse chemical-biology applications. *Chem. Rev.* **2013**, *113*, 4905–4979. [[CrossRef](#)] [[PubMed](#)]
17. Witczak, Z.J.; Bielski, R. *Click Chemistry in Glycoscience: New Developments and Strategies*; Wiley-VCH: Weinheim, Germany, 2013.

18. Goldmann, A.S.; Glassner, M.; Inglis, A.J.; Barner-Kowollik, C. Post-functionalization of polymers via orthogonal ligation chemistry. *Macromol. Rap. Commun.* **2013**, *34*, 810–849. [[CrossRef](#)] [[PubMed](#)]
19. Sreedhar, B.; Surendra Reddy, P. Sonochemical synthesis of 1,4-disubstituted 1,2,3-triazoles in aqueous medium. *Synth. Commun.* **2007**, *37*, 805–812. [[CrossRef](#)]
20. Cintas, P.; Martina, K.; Robaldo, B.; Garella, A.; Boffa, L.; Cravotto, G. Improved protocols for microwave-assisted Cu(I)-catalyzed Huisgen 1,3-dipolar cycloadditions. *Collect. Czech. Chem. Commun.* **2007**, *72*, 1014–1024. [[CrossRef](#)]
21. Cravotto, G.; Fokin, V.V.; Garella, D.; Binello, A.; Barge, A. Huisgen 1,3-dipolar cycloaddition catalyzed by metallic copper under ultrasound. *J. Comb. Chem.* **2010**, *12*, 13–15. [[CrossRef](#)] [[PubMed](#)]
22. Cintas, P.; Barge, A.; Tagliapietra, T.; Boffa, L.; Cravotto, G. Alkyne-azide click reaction catalyzed by metallic copper under ultrasound. *Nat. Protoc.* **2010**, *5*, 607–616. [[CrossRef](#)] [[PubMed](#)]
23. Klufers, P.; Piotrowski, H.; Uhlendorf, J. Homoleptic cuprates(II) with multiply deprotonated α -cyclodextrin ligands. *Chem. Eur. J.* **1997**, *3*, 601–608. [[CrossRef](#)]
24. Boffa, L.; Calcio Gaudino, E.; Martina, K.; Jicsinszky, L.; Cravotto, G. A new class of cationic cyclodextrins: Synthesis and chemico-physical properties. *New J. Chem.* **2010**, *34*, 2013–2019. [[CrossRef](#)]
25. Jacob, K.; Stolle, A.; Ondruschka, B.; Jandt, K.D.; Keller, T.F. Cu on porous glass: An easily recyclable catalyst for the microwave-assisted azide-alkyne cycloaddition in water. *Appl. Catal. A Gen.* **2013**, *451*, 94–100. [[CrossRef](#)]
26. Tu, N.P.; Hochlowski, J.E.; Djuric, S.W. Ultrasound-assisted click chemistry in continuous flow. *Mol. Divers.* **2012**, *16*, 53–58. [[CrossRef](#)] [[PubMed](#)]
27. Sreedhar, B.; Surendra Reddy, P.; Veda Prakash, B.; Ravindra, A. Ultrasound-assisted rapid and efficient synthesis of propargylamines. *Tetrahedron Lett.* **2005**, *46*, 7019–7022. [[CrossRef](#)]
28. Cargnelutti, R.; Lang, E.S.; Schumacher, R.F. Bis(2-pyridyl)diselenoethers as versatile ligands for copper-catalyzed C-S bond formation in glycerol. *Tetrahedron Lett.* **2015**, *56*, 5218–5222. [[CrossRef](#)]
29. Pirola, C.; Bianchi, C.L.; Di Michele, A.; Diodati, P.; Boffito, D.; Ragaini, V. Ultrasound and microwave assisted synthesis of high loading Fe-supported Fischer-Tropsch catalysts. *Ultrason. Sonochem.* **2010**, *17*, 610–616. [[CrossRef](#)] [[PubMed](#)]
30. Huang, W.; Li, H.; Zhu, B.; Feng, Y.; Wang, S.; Zhang, S. Selective hydrogenation of furfural to furfuryl alcohol over catalysts prepared via sonochemistry. *Ultrason. Sonochem.* **2007**, *14*, 67–74. [[CrossRef](#)] [[PubMed](#)]
31. Arena, F.; Italiano, G.; Barbera, K.; Bonura, G.; Spadaro, L.; Frusteri, F. Basic evidences for methanol-synthesis catalyst design. *Catal. Today* **2009**, *143*, 80–85. [[CrossRef](#)]
32. Shih-Yuan, A.; Dai, W.-C. A simple and highly efficient preparation of arylstannane(s) via sonochemical Barbier reaction. *Tetrahedron Lett.* **1996**, *37*, 495–498. [[CrossRef](#)]
33. Lee, A.S.-Y.; Dai, W.-C. A facile and highly efficient sonochemical synthesis of organostannane via Barbier reaction. *Tetrahedron* **1997**, *53*, 859–868. [[CrossRef](#)]
34. David-Quillot, F.; Lunot, S.; Marsacq, D.; Duchêne, A. A novel access to organogermanium compounds. *Tetrahedron Lett.* **2000**, *41*, 4905–4907. [[CrossRef](#)]
35. Lamandé-Langle, S.; Abarbri, M.; Thibonnet, J.; Duchêne, A. A novel mode of access to polyfunctional organotin compounds and their reactivity in Stille cross-coupling reaction. *J. Organomet. Chem.* **2009**, *694*, 2368–2374. [[CrossRef](#)]
36. Domini, C.E.; Silbestri, G.F.; Fernández Band, B.; Chopra, A.B. Ultrasound-assisted synthesis of unsymmetrical biaryls by Stille cross-coupling reactions. *Ultrason. Sonochem.* **2012**, *19*, 410–414. [[CrossRef](#)] [[PubMed](#)]
37. Lo Fiego, M.J.; Badajoz, M.A.; Domini, C.; Chopra, A.B.; Lockhart, M.T. Indium-mediated regioselective synthesis of ketones from arylstannanes under solvent free ultrasound irradiation. *Ultrason. Sonochem.* **2013**, *20*, 826–832. [[CrossRef](#)] [[PubMed](#)]
38. Cintas, P. Synthetic organoindium chemistry: What makes indium so appealing? *Synlett* **1995**, *1995*, 1087–1096. [[CrossRef](#)]
39. Shen, Z.-L.; Wang, S.-Y.; Chok, Y.-K.; Xu, Y.-H.; Loh, T.-P. Organoindium reagents: The preparation and application in organic synthesis. *Chem. Rev.* **2013**, *113*, 271–401. [[CrossRef](#)] [[PubMed](#)]
40. Cravotto, G.; Giovenzana, G.B.; Maspero, A.; Pilati, T.; Penoni, A.; Palmisano, G. Allylindation of 1H-indole-3-carboxaldehyde in the presence of azoles—revisited. *Tetrahedron Lett.* **2006**, *47*, 6439–6443. [[CrossRef](#)]
41. Cravotto, G.; Giovenzana, G.B.; Palmisano, G.; Penoni, A.; Pilati, T.; Sisti, M.; Stazi, F. Convolutamydine A: The first authenticated absolute configuration and enantioselective synthesis. *Tetrahedron Asymmetry* **2006**, *17*, 3070–3074. [[CrossRef](#)]

42. Colombo, F.; Cravotto, G.; Palmisano, G.; Penoni, A.; Sisti, M. 3-Component indium-mediated domino allylation of 1H-indole-3-carboxaldehyde with electron-rich (het)arenes: Highly efficient access to diversely functionalized indolylbutenes. *Eur. J. Org. Chem.* **2008**, *2008*, 2801–2807. [[CrossRef](#)]
43. Soengas, R.G.; Segade, Y.; Jiménez, C.; Rodríguez, J. Highly diastereoselective indium-mediated synthesis of β -lactam carbohydrates from imines. *Tetrahedron* **2011**, *67*, 2617–2622. [[CrossRef](#)]
44. Soengas, R.G. A straightforward route to novel α,α -disubstituted tetrahydrofuran β -amino acids and spirodiketopiperazines from sugar lactones. *Synlett* **2010**, *2010*, 2549–2552. [[CrossRef](#)]
45. Soengas, R.G.; Estévez, A.M. Indium-mediated allylation and Reformatsky reaction on glyoxylic oximes under ultrasound irradiation. *Ultrason. Sonochem.* **2012**, *19*, 916–920. [[CrossRef](#)] [[PubMed](#)]
46. Ishihara, J.; Watanabe, Y.; Koyama, N.; Nishino, Y.; Takahashi, K.; Hatakeyama, S. *Tetrahedron* **2011**, *67*, 3659–3667.
47. Cooper, B.F.T.; MacDonald, C.L.B. Alternative syntheses of univalent indium salts including a direct route from indium metal. *New J. Chem.* **2010**, *34*, 1551–1555. [[CrossRef](#)]
48. Downs, A.J.; Himmel, H.-J. New light on the chemistry of the group 13 metals. In *The Group 13 Metals Aluminium, Gallium, Indium and Thallium: Chemical Patterns and Peculiarities*, 1st ed.; Aldridge, S., Downs, A.J., Eds.; John Wiley & Sons, Ltd.: Chichester, UK, 2011; p. 1.
49. Araki, S.; Ito, H.; Butsugan, Y. Gallium-induced Barbier coupling of carbonyl compounds with allyl iodide. *Appl. Organomet. Chem.* **1988**, *2*, 475–478. [[CrossRef](#)]
50. Goswami, D.; Chattopadhyay, A.; Sharma, A.; Chattopadhyay, S. [Bmim][Br] as a solvent and activator for the Ga-mediated Barbier allylation: Direct formation of an N-heterocyclic carbene from Ga metal. *J. Org. Chem.* **2012**, *77*, 11064–11070. [[CrossRef](#)] [[PubMed](#)]
51. Qin, B.; Schneider, U. Catalytic use of elemental gallium for carbon-carbon bond formation. *J. Am. Chem. Soc.* **2016**, *138*, 13119–13122. [[CrossRef](#)] [[PubMed](#)]
52. Kumar, V.B.; Gedanken, A.; Kimmer, G.; Porat, Z. Ultrasonic cavitation of molten gallium: Formation of micro- and nano-spheres. *Ultrason. Sonochem.* **2014**, *21*, 1166–1173. [[CrossRef](#)] [[PubMed](#)]
53. Kumar, V.B.; Koltypin, Y.; Gedanken, A.; Porat, Z. Ultrasonic cavitation of molten gallium in water: Entrapment of organic molecules in gallium microspheres. *J. Mater. Chem. A* **2014**, *2*, 1309–1317. [[CrossRef](#)]
54. Shirazi, F.S.; Akhbari, K. Sonochemical procedures; the main synthetic methods for synthesis of coinage metal ion supramolecular polymer nanostructures. *Ultrason. Sonochem.* **2016**, *31*, 51–61. [[CrossRef](#)] [[PubMed](#)]
55. Rahmani, F.; Haghighi, M.; Mahboob, S. CO₂-enhanced dehydrogenation of ethane over sonochemically synthesized Cr/clinoptilolite-ZrO₂ nanocatalyst: Effects of ultrasound irradiation and ZrO₂ loading on catalytic activity and stability. *Ultrason. Sonochem.* **2016**, *33*, 150–163. [[CrossRef](#)] [[PubMed](#)]
56. Dai, Q.; Wang, J.; Yu, J.; Chen, J.; Chen, J. Catalytic ozonation for the degradation of acetylsalicylic acid in aqueous solution by magnetic CeO₂ nanometer catalyst particles. *Appl. Catal. B* **2014**, *144*, 686–693. [[CrossRef](#)]
57. Gobouri, A.A. Ultrasound enhanced photocatalytic properties of α -Fe₂O₃ nanoparticles for degradation of dyes used by textile industry. *Res. Chem. Intermed.* **2016**, *42*, 5099–5113. [[CrossRef](#)]
58. Ziyilan, A.; Ince, N.H. Catalytic ozonation of ibuprofen with ultrasound and Fe-based catalysts. *Catal. Today* **2014**, *240*, 5–8. [[CrossRef](#)]
59. Safari, J.; Gandomi-Ravandi, S. Application of the ultrasound in the mild synthesis of substituted 2,3-dihydroquinazolin-4(1H)-ones catalyzed by heterogeneous metal-MWCNTs nanocomposites. *J. Mol. Struct.* **2014**, *1072*, 173–178. [[CrossRef](#)]
60. Safari, J.; Zarnegar, Z. Biginelli reaction on Fe₃O₄-MWCNT nanocomposite: Excellent reactivity and facile recyclability of the catalyst combined with ultrasound irradiation. *RSC Adv.* **2013**, *3*, 17962–17967. [[CrossRef](#)]
61. Jiang, B.; Zhang, C.; Wang, K.; Dou, B.; Song, Y.; Chen, H.; Xu, Y. Highly dispersed Ni/montmorillonite catalyst for glycerol steam reforming: Effect of Ni loading and calcination temperature. *Appl. Therm. Eng.* **2016**, *109*, 99–108. [[CrossRef](#)]
62. Behling, R.; Chatel, G.; Valange, S. Sonochemical oxidation of vanillyl alcohol to vanillin in the presence of a cobalt oxide catalyst under mild conditions. *Ultrason. Sonochem.* **2017**, *36*, 27–35. [[CrossRef](#)] [[PubMed](#)]
63. Kim, A.; Sharma, B.; Kim, B.-S.; Park, K.H. Double-hydrophilic block copolymer nanoreactor for the synthesis of copper nanoparticles and for application in click chemistry. *J. Nanosci. Nanotechnol.* **2011**, *11*, 6162–6166. [[CrossRef](#)] [[PubMed](#)]

64. Stucchi, M.; Bianchi, C.L.; Pirola, C.; Cerrato, G.; Morandi, S.; Argirusis, C.; Sourkounie, G.; Naldonif, A.; Capucci, V. Copper NPs decorated titania: A novel synthesis by high energy US with a study of the photocatalytic activity under visible light. *Ultrason. Sonochem.* **2016**, *31*, 295–301. [[CrossRef](#)] [[PubMed](#)]
65. Astruc, D. Palladium nanoparticles as efficient green homogeneous and heterogeneous carbon-carbon coupling precatalysts: A unifying approach. *Inorg. Chem.* **2007**, *46*, 1884–1894. [[CrossRef](#)] [[PubMed](#)]
66. Zhang, Z.; Zha, Z.; Gan, C.; Pan, C.; Zhou, Y.; Wang, Z.; Zhou, M.-M. Catalysis and regioselectivity of the aqueous Heck reaction by Pd(0) nanoparticles under ultrasonic irradiation. *J. Org. Chem.* **2006**, *71*, 4339–4342. [[CrossRef](#)] [[PubMed](#)]
67. Gholap, A.R.; Venkatesan, K.; Pasricha, R.; Daniel, T.; Lahoti, R.J.; Srinivasan, K.V. Copper- and ligand-free Sonogashira reaction catalyzed by Pd(0) nanoparticles at ambient conditions under ultrasound irradiation. *J. Org. Chem.* **2005**, *70*, 4869–4872. [[CrossRef](#)] [[PubMed](#)]
68. Saliman, M.A.; Okawa, H.; Takai, M.; Ono, Y.; Kato, T.; Sugawara, K.; Sato, M. Improved battery performance using Pd nanoparticles synthesized on the surface of LiFePO₄/C by ultrasound irradiation. *Jpn. J. Appl. Phys.* **2016**, *55*, 07KE05. [[CrossRef](#)]
69. Ziylan-Yavas, A.; Mizukoshi, Y.; Maeda, Y.; Ince, N.H. Supporting of pristine TiO₂ with noble metals to enhance the oxidation and mineralization of paracetamol by sonolysis and sonophotolysis. *Appl. Catal. B* **2015**, *172*, 7–17. [[CrossRef](#)]
70. Kim, J.; Park, J.-E.; Momma, T.; Osaka, T. Synthesis of Pd-Sn nanoparticles by ultrasonic irradiation and their electrocatalytic activity for oxygen reduction. *Electrochim. Acta* **2009**, *54*, 3412–3418. [[CrossRef](#)]
71. Brancewicz, E.; Gradzka, E.; Basa, A.; Winkler, K. Chemical synthesis and characterization of the C60-Pd polymer spherical nanoparticles. *Electrochim. Acta* **2014**, *128*, 91–101. [[CrossRef](#)]
72. Tang, S.; Vongehr, S.; Zheng, Z.; Ren, H.; Meng, X. Facile and rapid synthesis of spherical porous palladium nanostructures with high catalytic activity for formic acid electro-oxidation. *Nanotechnology* **2012**, *23*, 255606. [[CrossRef](#)] [[PubMed](#)]
73. Estifae, P.; Haghighi, M.; Mohammadi, N.; Rahmani, F. CO oxidation over sonochemically synthesized Pd-Cu/Al₂O₃ nanocatalyst used in hydrogen purification: Effect of Pd loading and ultrasound irradiation time. *Ultrason. Sonochem.* **2014**, *21*, 1155–1165. [[CrossRef](#)] [[PubMed](#)]
74. Colmenares, J.C.; Magdziarz, A.; Łomot, D.; Chernyayeva, O.; Lisovytskiy, D. A new photocatalytic tool in VOCs abatement: Effective synergetic combination of sonication and light for the synthesis of monometallic palladium-containing TiO₂. *Appl. Catal. B* **2014**, *147*, 624–632. [[CrossRef](#)]
75. Colmenares, J.C.; Magdziarz, A. Method of Depositing Metal Nanoparticles on the Surface of Semiconductor Materials and Surface Obtained by this Process. Patent No. P.401693, 20 November 2012.
76. Colmenares, J.C.; Lisowski, P.; Łomot, D.; Chernyayeva, O.; Lisovytskiy, D. Sonophotodeposition of bimetallic photocatalysts Pd-Au/TiO₂: Application to selective oxidation of methanol to methyl formate. *ChemSusChem* **2015**, *8*, 1676–1685. [[CrossRef](#)] [[PubMed](#)]
77. Basavegowda, N.; Mishra, K.; Lee, Y.R. Ultrasonic-assisted green synthesis of palladium nanoparticles and their nanocatalytic application in multicomponent reaction. *New J. Chem.* **2015**, *39*, 972–977. [[CrossRef](#)]
78. Colmenares, J.C.; Aramendía, M.A.; Marinas, A.; Marinas, J.M.; Urbano, F.J. Synthesis, characterization and photocatalytic activity of different metal-doped titania systems. *Appl. Catal. A Gen.* **2006**, *306*, 120–127. [[CrossRef](#)]
79. Aramendía, M.A.; Colmenares, J.C.; Marinas, A.; Marinas, J.M.; Moreno, J.M.; Navío, J.A.; Urbano, F.J. Effect of the redox treatment of Pt/TiO₂ system on its photocatalytic behaviour in the gas phase selective photooxidation of propan-2-ol. *Catal. Today* **2007**, *128*, 235–244. [[CrossRef](#)]
80. Colmenares, J.C.; Aramendia, M.A.; Marinas, A.; Marinas, J.M.; Urbano, F.J. Titania nano-photocatalysts synthesized by ultrasound and microwave methodologies: Application in depuration of water from 3-chloropyridine. *J. Mol. Catal. A Chem.* **2010**, *331*, 58–63. [[CrossRef](#)]
81. López-Tenllado, F.J.; Marinas, A.; Urbano, F.J.; Colmenares, J.C.; Hidalgo, M.C.; Marinas, J.M.; Moreno, J.M. Selective photooxidation of alcohols as test reaction for photocatalytic activity. *Appl. Catal. B* **2012**, *128*, 150–158. [[CrossRef](#)]
82. Vinodgopal, K.; Neppolian, B.; Salleh, N.; Lightcap, I.V.; Grieser, F.; Ashokkumar, M.; Ding, T.T.; Kamat, P.V. Dual-frequency ultrasound for designing two dimensional catalyst surface: Reduced graphene oxide-Pt composite. *Coll. Surf. A* **2012**, *409*, 81–87. [[CrossRef](#)]

83. Cravotto, G.; Cintas, P. Sonication-assisted fabrication and post-synthetic modifications of graphene-like materials. *Chem. Eur. J.* **2010**, *16*, 5246–5259. [[CrossRef](#)] [[PubMed](#)]
84. Ciesielski, A.; Samori, P. Graphene via sonication assisted liquid-phase exfoliation. *Chem. Soc. Rev.* **2014**, *43*, 381–398. [[CrossRef](#)] [[PubMed](#)]
85. Toukoniitty, B.; Toukoniitty, E.; Mäki-Arvela, P.; Mikkola, J.-P.; Salmi, T.; Murzin, D.Y.; Kooyman, P.J. Effect of ultrasound in enantioselective hydrogenation of 1-phenyl-1,2-propanedione: Comparison of catalyst activation, solvents and supports. *Ultrason. Sonochem.* **2006**, *13*, 68–75. [[CrossRef](#)] [[PubMed](#)]
86. Perkas, N.; Rotter, H.; Vradman, L.; Landau, M.V.; Gedanken, A. Sonochemically prepared Pt/CeO₂ and its application as a catalyst in ethyl acetate combustion. *Langmuir* **2006**, *22*, 7072–7077. [[CrossRef](#)] [[PubMed](#)]
87. Selvaraj, V.; Alagar, M. Ethylene glycol oxidation on Pt and Pt-Ru nanoparticle decorated polythiophene/multiwalled carbon nanotube composites for fuel cell applications. *Nanotechnology* **2008**, *19*, 045504. [[CrossRef](#)] [[PubMed](#)]
88. Jang, J.-H.; Kim, J.; Lee, Y.-H.; Kim, I.Y.; Park, M.-H.; Yang, C.-W.; Hwang, S.-J.; Kwon, Y.-U. One-pot synthesis of core-shell-like Pt₃Co nanoparticle electrocatalyst with Pt-enriched surface for oxygen reduction reaction in fuel cells. *Energy Environ. Sci.* **2011**, *4*, 4947–4953. [[CrossRef](#)]
89. Jiang, R.; Rong, C.; Chu, D. Surface coverage of Pt atoms on PtCo nanoparticles and catalytic kinetics for oxygen reduction. *Electrochim. Acta* **2011**, *56*, 2532–2540. [[CrossRef](#)]
90. Nagao, D.; Shimazaki, Y.; Saeki, S.; Kobayashi, Y.; Konno, M. Effect of ultrasonic irradiation on carbon-supported Pt-Ru nanoparticles prepared at high metal concentration. *Coll. Surf. A* **2007**, *302*, 623–627. [[CrossRef](#)]
91. Ruiz-Camacho, B.; Álvarez, O.M.; Rodríguez-Santoyo, H.H.; López-Peréz, P.A.; Fuentes-Ramírez, R. Mono and bi-metallic electrocatalysts of Pt and Ag for oxygen reduction reaction synthesized by sonication. *Electrochem. Commun.* **2015**, *61*, 5–9. [[CrossRef](#)]
92. Cinelli, M.; Coles, S.R.; Nadagouda, M.N.; Blaszczyński, J.; Slowiński, R.; Varma, R.S.; Kirwan, K. A green chemistry-based classification model for the synthesis of silver nanoparticles. *Green Chem.* **2015**, *17*, 2825–2839. [[CrossRef](#)]
93. Chernousova, S.; Epple, M. Silver as antibacterial agent: Ion, nanoparticle, and metal. *Angew. Chem. Int. Ed.* **2013**, *52*, 1636–1653. [[CrossRef](#)] [[PubMed](#)]
94. Manjamadha, V.P.; Muthukumar, K. Ultrasound assisted green synthesis of silver nanoparticles using weed plant. *Bioprocess Biosyst. Eng.* **2016**, *39*, 401–411. [[CrossRef](#)] [[PubMed](#)]
95. Sun, L.; Li, J.; Wang, C.; Li, S.; Lai, Y.; Chen, H.; Lin, C. Ultrasound aided photochemical synthesis of Ag loaded TiO₂ nanotube arrays to enhance photocatalytic activity. *J. Hazard. Mater.* **2009**, *171*, 1045–1050. [[CrossRef](#)] [[PubMed](#)]
96. Jhuang, Y.Y.; Cheng, W.T. Fabrication and characterization of silver/titanium dioxide composite nanoparticles in ethylene glycol with alkaline solution through sonochemical process. *Ultrason. Sonochem.* **2016**, *28*, 327–333. [[CrossRef](#)] [[PubMed](#)]
97. Pech-Pech, I.E.; Gervasio, D.F.; Godínez-García, A.; Solorza-Feria, O.; Pérez-Robles, J.F. Nanoparticles of Ag with a Pt and Pd rich surface supported on carbon as a new catalyst for the oxygen electroreduction reaction (ORR) in acid electrolytes: Part 1. *J. Power Sources* **2015**, *276*, 365–373. [[CrossRef](#)]
98. Pech-Pech, I.E.; Gervasio, D.F.; Pérez-Robles, J.F. Nanoparticles of Ag with a Pt and Pd rich surface supported on carbon as a new catalyst for the oxygen electroreduction reaction (ORR) in acid electrolytes: Part 2. *J. Power Sources* **2015**, *276*, 374–381. [[CrossRef](#)]
99. Vu, T.A.; Dao, C.D.; Hoang, T.T.T.; Dang, P.T.; Tran, H.T.K.; Nguyen, K.T.; Le, G.H.; Nguyen, T.V.; Lee, G.D. Synthesis of novel silver vanadates with high photocatalytic and antibacterial activities. *Mater. Lett.* **2014**, *123*, 176–180. [[CrossRef](#)]
100. Lei, Z.; Zhang, L.; Wei, X. One-step synthesis of silver nanoparticles by sonication or heating using amphiphilic block copolymer as templates. *J. Coll. Interface Sci.* **2008**, *324*, 216–219. [[CrossRef](#)] [[PubMed](#)]
101. Saha, S.K.; Roy, P.; Saini, P.; Mondal, M.K.; Chowdhury, P.; Babu, S.P.S. Carbohydrate polymer inspired silver nanoparticles for filaricidal and mosquitocidal activities: A comprehensive view. *Carbohydr. Polym.* **2016**, *137*, 390–401. [[CrossRef](#)] [[PubMed](#)]
102. Kuo, T.-C.; Hsu, T.-C.; Liu, Y.-C.; Yang, K.-H. Size-controllable synthesis of surface-enhanced Raman scattering-active gold nanoparticles coated on TiO₂. *Analyst* **2012**, *137*, 3847–3853. [[CrossRef](#)] [[PubMed](#)]

103. Wen, B.; Ma, J.; Chen, C.; Ma, W.; Zhu, H.; Zhao, J. Supported noble metal nanoparticles as photo/sono-catalysts for synthesis of chemicals and degradation of pollutants. *Sci. China Chem.* **2011**, *54*, 887–897. [[CrossRef](#)]
104. George, P.P.; Gedanken, A.; Perkas, N.; Zhong, Z. Selective oxidation of CO in the presence of air over gold-based catalysts Au/TiO₂/C (sonochemistry) and Au/TiO₂/C (microwave). *Ultrason. Sonochem.* **2008**, *15*, 539–547. [[CrossRef](#)] [[PubMed](#)]
105. Mizukoshi, Y.; Makise, Y.; Shuto, T.; Hu, J.; Tominaga, A.; Shironita, S.; Tanabe, S. Immobilization of noble metal nanoparticles on the surface of TiO₂ by the sonochemical method: Photocatalytic production of hydrogen from an aqueous solution of ethanol. *Ultrason. Sonochem.* **2007**, *14*, 387–392. [[CrossRef](#)] [[PubMed](#)]
106. Kan, C.; Zhu, J.; Wang, C. Ag nanoparticle-filled polymer shell formed around Au nanoparticle core via ultrasound-assisted spherulite growth. *J. Cryst. Growth* **2009**, *311*, 1565–1570. [[CrossRef](#)]
107. Park, J.-E.; Atobe, M.; Fuchigami, T. Sonochemical synthesis of conducting polymer-metal nanoparticles nanocomposite. *Electrochim. Acta* **2005**, *51*, 849–854. [[CrossRef](#)]
108. Fang, Y.; Li, X.; Hu, Y.; Li, F.; Lin, X.; Tian, M.; Anc, X.; Fud, Y.; Jina, J.; Ma, J. Ultrasonication-assisted ultrafast preparation of multiwalled carbon nanotubes/Au/Co₃O₄ tubular hybrids as superior anode materials for oxygen evolution reaction. *J. Power Sources* **2015**, *300*, 285–293. [[CrossRef](#)]
109. Yusof, N.S.M.; Ashokkumar, M. Sonochemical synthesis of gold nanoparticles by using high intensity focused ultrasound. *ChemPhysChem* **2015**, *16*, 775–781. [[CrossRef](#)] [[PubMed](#)]
110. Vilela, S.M.F.; Ananias, D.; Fernandes, J.A.; Silva, P.; Gomes, A.C.; Silva, N.J.O.; Rodrigues, M.O.; Tomé, J.P.C.; Valente, A.A.; Ribeiro-Claro, P.; et al. Multifunctional micro- and nanosized metal-organic frameworks assembled from bisphosphonates and lanthanides. *J. Mater. Chem. C* **2014**, *2*, 3311–3327. [[CrossRef](#)]
111. Amith Yadav, H.J.; Eraiah, B.; Nagabhushana, H.; Darshan, G.P.; Daruka Prasad, B.; Sharma, S.C.; Premkumar, H.B.; Anantharaju, K.S.; Vijayakumar, G.R. Facile ultrasound route to prepare micro/nano superstructures for multifunctional applications. *ACS Sust. Chem. Eng.* **2017**, *5*, 2061–2074. [[CrossRef](#)]
112. Gottapu, S.; Padhi, S.K.; Krishna, M.G.; Muralidharan, K. Poly(vinylpyrrolidone) stabilized aluminum nanoparticles obtained by the reaction of SiCl₄ with LiAlH₄. *New J. Chem.* **2015**, *39*, 5203–5207. [[CrossRef](#)]
113. Kumar, V.B.; Mastai, Y.; Porat, Z.; Gedanken, A. Chiral imprinting in molten gallium. *New J. Chem.* **2015**, *39*, 2690–2696. [[CrossRef](#)]
114. Nissan, I.; Kumar, V.B.; Porat, Z.; Makovec, D.; Shefi, O.; Gedanken, A. Sonochemically-fabricated Ga@C-dots@Ga nanoparticle-aided neural growth. *J. Mater. Chem. B* **2017**, *5*, 1371–1379. [[CrossRef](#)]
115. Safari, J.; Gandomi-Ravandi, S.; Akbari, Z. Sonochemical synthesis of 1,2,4,5-tetrasubstituted imidazoles using nanocrystalline MgAl₂O₄ as an effective catalyst. *J. Adv. Res.* **2013**, *4*, 509–514. [[CrossRef](#)] [[PubMed](#)]



© 2017 by the authors. Licensee MDPI, Basel, Switzerland. This article is an open access article distributed under the terms and conditions of the Creative Commons Attribution (CC BY) license (<http://creativecommons.org/licenses/by/4.0/>).